Title

Executioner caspase is proximal to Fasciclin 3 which facilitates non-lethal activation in *Drosophila* olfactory receptor neurons

Short title

Fasciclin 3 non-lethally activates caspase in *Drosophila* olfactory neurons

Authors

Masaya Muramoto[a,1], Nozomi Hanawa[a,1], Misako Okumura[b,c], Takahiro Chihara[b,c], Masayuki Miura[a,2], and Natsuki Shinoda[a,2]

Affiliations & Footnotes

[a]Department of Genetics, Graduate School of Pharmaceutical Sciences, University of Tokyo, 7-3-1 Hongo, Bunkyo-ku, Tokyo 113-0033, Japan

[b]Program of Biomedical Science, Graduate School of Integrated Sciences for Life, Hiroshima University, Higashi-Hiroshima, Hiroshima 739-8526, Japan

[c]Program of Basic Biology, Graduate School of Integrated Sciences for Life, Hiroshima University, Higashi-Hiroshima, Hiroshima 739-8526, Japan

[1]Equal contributions

[2]Corresponding authors

Corresponding Authors

Masayuki Miura: Department of Genetics, Graduate School of Pharmaceutical Sciences, University of Tokyo, 7-3-1 Hongo, Bunkyo-ku, Tokyo 113-0033, Japan. Telephone: +81-3-5841-4860. E-mail: miura@mol.f.u-tokyo.ac.jp

Natsuki Shinoda: Department of Genetics, Graduate School of Pharmaceutical Sciences, University of Tokyo 7-3-1 Hongo, Bunkyo-ku, Tokyo 113-0033, Japan. Telephone: +81-3-5841-4867. E-mail: f-shinoda.natsuki@g.ecc.u-tokyo.ac.jp

Author Contributions

Masaya Muramoto: Formal Analysis, Investigation, Methodology, Resources, Writing – Review & Editing; Nozomi Hanawa: Formal analysis, Investigation, Methodology, Resources, Writing – Review & Editing; Misako Okumura: Methodology, Writing – Review & Editing; Takahiro Chihara: Methodology, Writing – Review & Editing; Masayuki Miura: Conceptualization, Funding Acquisition, Supervision, Writing – Original Draft Preparation; Natsuki Shinoda: Conceptualization, Formal Analysis, Funding Acquisition, Investigation, Project Administration, Supervision, Validation, Visualization, Writing – Original Draft Preparation

Conflict of Interest

The authors declare that they have no conflict of interest.

Abstract

Executioner caspases are activated by initiator caspases, resulting in lethal and non-lethal cellular outcomes. Despite the identification of numerous caspase-dependent non-lethal cellular processes (CDPs), the molecular mechanism that enables precise regulation of the non-lethal functions of executioner caspases remains unclear. Here, we conducted a comprehensive analysis of endogenous proximal proteins of *Drosophila* executioner caspases *in vivo* using TurboID. We discovered that in the adult brain, the executioner caspase Drice is, as an inactive proform, primarily proximal to cell membrane proteins, including the cell adhesion molecule Fasciclin 3 (Fas3). Notably, Drice is proximal to the specific alternative splicing isoforms of Fas3, Fas3G. To investigate whether Fas3G modulates caspase activity, we developed a Gal4-Manipulated Area-Specific CaspaseTracker/CasExpress (MASCaT) system for highly sensitive monitoring of non-lethal caspase activity near cell membrane compartments. Using MASCaT, we demonstrated that *Fas3G* overexpression promotes caspase activation near cell membrane compartments in olfactory receptor neurons without killing them. Mechanistically, *Fas3G* overexpression induces the expression of initiator caspase Dronc, which also comes close to Fas3G, regulating non-lethal caspase activation. Physiologically, *Fas3G* overexpression-facilitated caspase activation regulates innate olfactory attraction behavior. Collectively, our findings suggest that caspase activation is subcellularly restricted, the platform of which is defined by caspase proximal proteins, for non-lethal functions.

Author Summary

Caspases are Cysteine-ASPartic acid proteASEs which are primarily involved in cell death. In addition, caspases play versatile non-lethal (non-cell death) roles in a wide range of cell types including neurons. However, the molecular mechanism that enables the precise regulation of non-lethal activation and functions remains unclear. Here, we focused on the proximal proteins of caspases as potential regulators of non-lethal activation. By comprehensively analyzing the proximal proteins of caspases in the adult *Drosophila* brain using TurboID, we discovered that caspases are primarily proximal to membrane proteins rather than to cytosolic proteins. By developing a genetic tool that enables highly sensitive monitoring of non-lethal caspase activity near membrane compartments, we found that proximal proteins facilitate non-lethal caspase activation in olfactory receptor neurons. Importantly, non-lethal caspase activation in olfactory receptor neurons affects organismal innate attraction behavior. Our research suggests that a caspase activation is compartmentalized, the platform of which is defined by caspase proximal proteins, for non-lethal functions.

75 **Introduction**

76 Caspases are cysteine aspartic acid proteases involved in cell death. Apoptotic stimuli activate
77 initiator caspases that trigger a proteolytic cascade, leading to the activation of executioner
78 caspases and culminating in apoptosis (Fig. 1A) [1]. Caspases exhibit diverse non-lethal cellular
79 functions [2]. In the nervous system, non-lethal caspase activity promotes the maturation of
80 olfactory sensory neurons during development [3]. Furthermore, non-lethal caspase activity
81 induces long-term depression through AKT cleavage [4]. These are termed caspase-dependent
82 non-lethal cellular processes (CDPs) [5]. Despite the discovery of numerous CDPs over the past
83 two decades, the molecular mechanism that underlies specific non-lethal functions without
84 causing cell death remains unclear.

85 Proteins that interact with initiator caspases are among the key regulators of CDPs.
86 Tango7, the *Drosophila* translation initiation factor eIF3 subunit m, acts as an adapter and
87 regulates the localization of the initiator caspase Dronc. During sperm individualization,
88 Tango7 directs Dronc to the individualization complex [6]. In salivary glands, Tango7 directs
89 Dronc to the plasma membrane [7]. In both cases, caspase activity promotes cellular remodeling
90 without inducing cell death [6,7]. CRINKLED, a *Drosophila* unconventional myosin, functions
91 as an adaptor of Dronc and facilitates the cleavage of Shaggy46 [8]. Shaggy46, activated by
92 caspase-mediated cleavage, suppresses the emergence of ectopic sensory organ precursors [9].
93 During apoptosis-induced proliferation (AiP), Myo1D, another *Drosophila* unconventional
94 myosin, facilitates Dronc translocation to the basal side of the plasma membrane of imaginal
95 discs to promote AiP [10]. Thus, initiator caspase-interacting proteins regulate caspase activity
96 in CDPs. However, given the importance of executioner caspases, which cleave a broad range
97 of substrates and are essential for apoptosis [11,12], little is known about the subcellular
98 compartmentalization and interacting proteins of those involved in CDPs. This lack of

99 understanding is partly due to the absence of protein-protein interaction domains (e.g., DED
100 and CARD) in the N-terminus of executioner caspases [13].

101 To understand the molecular mechanism regulating caspase activity involved in CDPs,
102 we focused on the proximal proteins of executioner caspases using TurboID, a proximity
103 labeling technique that analyzes protein proximity *in vivo* [14,15]. We previously established
104 C-terminal TurboID knocked-in caspase fly lines for Dronc, Drice, and Dcp-1 [16]. Importantly,
105 we have demonstrated that one of the preferred substrates of Drice, BubR1, is proximal to Drice
106 *in vivo* [17], suggesting that substrate preference is exploited by protein proximity. Therefore,
107 the proximity of executioner caspases to proteins is emerging as a means of regulating specific
108 non-lethal functions.

109 In this study, through a comprehensive analysis of proximal proteins, we discovered
110 that the cell adhesion molecule Fasciclin 3 (Fas3) is in close proximity to the executioner
111 caspase Drice, as an inactive proform, in the adult brain. We observed that Drice was
112 exclusively proximal to specific alternative splicing isoforms of Fas3, Fas3G. To ascertain
113 whether Fas3G modulates caspase activity, we developed a Gal4-Manipulated Area Specific
114 CaspaseTracker/CasExpress (MASCaT) system, which permits the monitoring of caspase
115 activity with high sensitivity and simultaneous genetic manipulation in the cells of interest.
116 Using MASCaT, we demonstrated that *Fas3G* overexpression enhances caspase activation
117 without killing cells through the induction of the expression of initiator caspase Dronc, which
118 comes proximal to Fas3G. Subsequently, we showed that *Fas3G* overexpression-facilitated
119 activation regulates innate olfactory attraction behavior. Collectively, our findings suggest that
120 caspase activation is subcellularly restricted, the platform of which is defined by caspase
121 proximal proteins, for non-lethal functions.

122 **Results**

123 ***Drice is the major executioner caspase expressed in the adult brains***

124 In *Drosophila*, the caspase-mediated apoptotic signaling pathway is highly conserved [2]. The
125 activity of executioner caspases, specifically Drice and Dcp-1, is regulated by apoptotic
126 signaling pathways, including the initiator caspase Dronc (Fig. 1A). To investigate the
127 expression patterns of *Drosophila* caspases, we employed *Caspase::V5::TurboID* knocked-in
128 fly lines [16]. We found low levels of expression of the initiator caspase Dronc in adult heads
129 (Fig. 1B). Conversely, we observed high expression of the executioner caspase Drice, whereas
130 Dcp-1 was expressed at lower levels in adult heads (Fig. 1B). The proximal proteins of each
131 caspase were labeled with TurboID in adult heads by administration of 100 μM biotin (Fig. 1B).
132 Furthermore, we investigated the expression patterns of caspases using histochemical analysis
133 by examining streptavidin (SA) signal. Consistent with the western blotting findings, Drice
134 showed higher expression levels than Dronc and Dcp-1, which were expressed at lower levels
135 (Fig. 1C). We found that Drice was expressed in distinct regions, including the mushroom
136 bodies (MBs), suboesophageal ganglions (SGs), optic lobes (OLs), and antennal lobes (ALs),
137 which showed the highest levels of expression (Fig. 1C). The *Drosophila* ALs comprise
138 synaptic contacts between the axons of olfactory receptor neurons (ORNs), the dendrites of
139 projection neurons (PNs), and local interneuron (LNs) processes. Neuron-type-specific Gal4s
140 were used to knockdown *Drice* and the expression patterns were subsequently examined. We
141 found that Drice was expressed predominantly in ORNs in the AL (Fig. 1D). These results
142 showcase that Drice is not expressed in the entire brain, but rather in a specific subset of neurons
143 in the adult brains. Comparisons of the expression patterns of Drice were consistent across both
144 males and females (Fig. S1A), indicating an absence of sex-based differences, which justifies
145 the use of males for functional simplicity in this study.

146

147 ***Drice is proximal to cell membrane proteins rather than cytosolic proteins in the adult brains***

148 To comprehensively identify proximal proteins of Drice, we employed a proximity labeling
149 approach. Specifically, we used *Drice::V5::TurboID* knocked-in flies fed 100 μM biotin. We
150 confirmed biotinylation of Drice proximal proteins in the adult brains (Fig. 1E). After purifying
151 the biotinylated proteins using NeutrAvidin magnetic beads, we performed LC-MS/MS
152 analysis of the samples (Fig. 1F). We identified 643 proteins (Fig. 1G, Table S1), of which 158
153 were highly specific to *Drice::V5::TurboID* flies compared to wild-type flies
154 (*Drice::V5::TurboID*/w^{1118} > 10; Fig. 1G, Table S1). Gene ontology analysis revealed that
155 Drice proximal proteins were enriched in the plasma membrane, synaptic vesicles, postsynaptic
156 membranes, and adherens junctions (Fig. 1H, Table S2). This finding suggests that Drice is
157 localized primarily in cell membrane compartments rather than in the cytoplasm of the adult
158 brain. Additionally, because the SA signal of *Drice::V5::TurboID* is mainly observed in the
159 AL where the axons of ORNs project (Fig. 1C), the enrichment of cell membrane proteins in
160 the proximal proteins of Drice is reasonable.

161

162 ***A specific splicing isoform of Fasciclin 3 is in proximity to Drice***

163 During our analysis of proteins proximal to Drice, we discovered that the expression patterns
164 of Fasciclin 3 (Fas3) in the adult brain closely resembled those of Drice, especially within the
165 OLs, SGs, and ALs (Fig. 2A, B). Thus, we focused on Fas3 [18], a transmembrane protein
166 containing immunoglobulin-like domains that regulates synaptic target recognition and axon
167 fasciculation [19]. *Fas3* is encoded by seven splicing isoforms, resulting in the production of
168 five protein isoforms that share extracellular domains but differ in intracellular domains with
169 low-complexity sequences (Fig. 2C, D). Only one specific protein isoform, Fas3 isoform G
170 (Fas3G), was identified in the LC-MS/MS analysis as a Drice proximal protein in the adult
171 brain (Fig. 1G, Table S1). To validate this result, we generated an antibody specific to Fas3G

172 (Fig. 2C, E). We confirmed that only the Fas3G was labeled with Drice::V5::TurboID and
173 purified using NeutrAvidin magnetic beads as detected using western blotting (Fig. 2F). To
174 further confirm the isoform specificity to Drice proximity, we overexpressed 3xFLAG-tagged
175 *Fas3 isoforms A*, *B/F*, *C*, *D/E*, and *G* in olfactory receptor neurons using *Pebbled-Gal4* in a
176 *Drice::V5::TurboID* knocked-in background. After proximity labeling with TurboID, followed
177 by NeutrAvidin purification, we found that the Fas3G was highly enriched compared to the
178 other isoforms (Fig. 2G). These findings suggested that Drice is proximal to a specific isoform
179 of Fas3 in olfactory receptor neurons, regardless of its protein expression level. We also
180 investigated whether Drice and Fas3G physically interact by co-immunoprecipitation.
181 Although Fas3G was labelled by Drice::V5::TurboID, indicating its proximity to Drice within
182 the ORNs of adult brains, Drice did not co-immunoprecipitate with Fas3G (Fig. S2A). This
183 suggests that while Drice and Fas3G are proximate, they do not physically interact, highlighting
184 the utility of proximity labeling as a superior technique to conventional co-immunoprecipitation
185 for identifying proteins that are spatially close.
186
187 ***Fasciclin 3s are not substrates of caspase***
188 It is often observed that proteins in close proximity to caspases are their preferred substrates
189 [17]. To investigate this, we examined whether any of the Fas3 isoforms are substrates for
190 caspase by expressing all isoforms in *Drosophila* S2 cells. However, we found that none of the
191 Fas3 isoforms were cleaved by caspase following the induction of apoptosis (Fig. S2B).
192 Therefore, Fas3s are not substrates of caspase.
193
194 ***MASCaT: a cell type-specific highly sensitive non-lethal caspase activity reporter***
195 We investigated whether Fas3G regulates caspase activity in lethal or non-lethal processes.
196 CaspaseTracker/CasExpress is a highly sensitive reporter of non-lethal caspase activity that

197 uses caspase-activatable Gal4 tethered to the membrane by mCD8 [20,21]. However, reliance
198 on Gal4 to report their activity presents a challenge in reconciling Gal4/UAS-dependent gene
199 manipulations. To overcome this limitation, we created a new reporter to capture non-lethal
200 caspase activation independent of caspase-activatable Gal4. We replaced the caspase-
201 activatable Gal4 with the caspase-activatable QF2 (*mCD8::DQVD::QF2*), where DQVD is a
202 caspase cleavage sequence, and first expressed directly downstream of *UAS* sequence (Fig.
203 S3A). However, the caspase-activatable QF2 induced mNeonGreen expression under *QUAS*
204 sequence even either with a pan-caspase inhibitor, zVAD-fmk, or an uncleavable DQVA
205 mutant probe (*mCD8::DQVA::QF2*, insensitive to caspase-mediated cleavage which serves as
206 a negative control) (Fig. S3B), potentially because the Gal4/UAS binary system expressed
207 excessive mCD8::DQVD/A::QF2 probes that results in caspase activation-independent
208 induction of QF2/QUAS system. Thus, to reduce the amount of probes expression, we
209 generated *Ubi-FRT-STOP-FRT-mCD8::DQVD::QF2*, simultaneously expressing *Flippase*
210 (*FLP*) under *UAS* to restrict reporter expression to the cells of interest (Fig. 3A). *Drosophila* S2
211 cells undergo weak caspase activation only by transfection [17]. Taking advantage of that, this
212 system reports caspase activity through the caspase-activatable QF2/QUAS system, expressing
213 mNeonGreen, which is not detected by caspase-non-activatable QF2 (Fig. 3B). We named this
214 novel reporter a Gal4-Manipulated Area Specific CaspaseTracker/CasExpress (MASCaT; Fig.
215 3A). Utilizing MASCaT, we detected non-lethal caspase activity, specifically in the neurons of
216 adult brains, using *ELAV-Gal4* (Fig. 3C). Caspase activity was prominent in OLs (Fig. 3C),
217 which is consistent with the previously reported activation pattern of caspase detected by
218 CaspaseTracker/CasExpress [20,21]. Previously, we reported that a specific subset of ORNs,
219 including Or42b, undergoes age-associated caspase activation [22]. Consistent with this finding,
220 we detected age-dependent caspase activation in the AL (Fig. 3C). Therefore, our newly
221 established reporter, MASCaT, enables the highly sensitive detection of caspase activity near

222 the cell membrane in cells of interest reconciling with Gal4/UAS-dependent gene
223 manipulations.
224
225 ***Fas3G overexpression activates caspase in a non-lethal manner***
226 To investigate the regulatory role of Fas3 in caspase activity *in vivo*, we used Or42b neurons as
227 a model, which have previously been shown to undergo age-dependent caspase activation [22].
228 Initially, we evaluated the effects of *Dronc* overexpression on apoptosis by quantifying cell
229 body numbers in the antenna in young flies. Dronc induced cell loss while catalytically inactive
230 Dronc ($Dronc^{CG}$) did not, suggesting that Dronc induce apoptosis in a catalytic-dependent
231 manner (Fig. 4A, B). We then evaluated the effects of the overexpression of the executioner
232 caspases *Dcp-1* and *Drice*. Interestingly, although Dcp-1 induced complete cell loss, Drice did
233 not (Fig. 4A, B), suggesting that Drice requires an initiator caspase for activation, whereas Dcp-
234 1 does not. These results indicate that Or42b neurons are competent in caspase-mediated cell
235 loss and thus serve as a model for evaluating apoptosis. However, the expression of *Fas3G*,
236 even in combination with *Drice*, did not reduce the number of cells, implying that *Fas3G*
237 overexpression did not induce apoptosis (Fig. 4C, D).
238 Subsequently, we assessed the regulation of non-lethal caspase activity by Fas3G *in*
239 *vivo*. We first confirmed that MASCaT probes were distributed in the axons of ORNs (Fig. 4E).
240 Using MASCaT, we observed weak non-lethal caspase activation even in the control group at
241 a young age (Fig. 4F, G). The expression of *Fas3G* significantly promoted caspase activation
242 (Fig. 4F, G), indicating that Fas3G regulates non-lethal caspase activation. Moreover, the
243 simultaneous expression of *Drice* and *Fas3G* significantly enhanced caspase activation (Fig.
244 4F, G), signifying the promoting effect of their proximity. Moreover, the concurrent expression
245 of Diap-1, an E3 ligase known to inhibit caspase activation [23–25], mitigated the caspase
246 activation induced by Fas3G overexpression (Fig. 4H, I). This indicates that *Fas3G*

247 overexpression-facilitated non-lethal caspase activation is dependent on the core apoptotic
248 machinery. To test whether endogenous Fas3G regulates caspase activation, we generated
249 *Fas3G*-specific *shRNA* expressing strain (Fig. S4A, B). Knockdown of *Fas3* or *Fas3G* in Or42b
250 neurons didn't suppress the inherent, weak caspase activation (Fig. S4C, D). In agreement with
251 this, Drice's presence in the axon of ORNs with Fas3G was observed, yet its presence was not
252 strictly contingent on Fas3 or Fas3G (Fig. S4E). Given the numerous other membrane proteins
253 in proximity to Drice (Fig. 1G, H and Table S1), it is probable that additional proteins may be
254 responsible for recruiting Drice to the axon. These findings collectively imply that while Fas3G
255 is not essential for mild endogenous caspase activation, overexpression of *Fas3G* does enhance
256 non-lethal caspase activation in ORNs, thus providing a valuable model for exploring the
257 molecular processes that facilitate caspase activation without leading to cell death.
258
259 ***Fas3G is proximal to Dronc which is required for non-lethal caspase activation***
260 Next, we investigated the underlying mechanism that enhances non-lethal activation facilitated
261 by *Fas3G* overexpression. Executioner caspases, Drice and Dcp-1, are activated by initiator
262 caspases, Dronc (Fig. 1A). We precisely analyzed Dronc's expression pattern in adult brains
263 and found that while its expression was low in control, overexpression of *Fas3G* in ORNs
264 markedly increased Dronc levels in those neurons (Fig. 5A). Moreover, akin to Drice, Dronc
265 was also found in close proximity to the overexpressed Fas3G, but not to the overexpressed
266 Fas3C in ORNs (Fig. 5B). Consequently, we examined whether Dronc is required for the non-
267 lethal caspase activation enhanced by *Fas3G* overexpression. Employing MASCaT, we
268 discovered that both knockdown of *Dronc* and the expression of the dominant-negative form
269 of *Dronc* hindered the non-lethal caspase activation facilitated by *Fas3G* overexpression (Fig.
270 5C, D), indicating a dependence on initiator caspase activity. Importantly1, the genetic
271 suppression of Dronc activity did not alter the proximity between Drice and Fas3G (Fig. 5E),

272 suggesting that the inactive Drice proform is naturally near Fas3G. Solo overexpression of
273 *Dronc* led to cell death in Or42b neurons (Fig. 4A, B), whereas *Fas3G* overexpression elevated
274 Dronc expression without causing cell death (Fig. 4C, D, Fig. 5A). Collectively, these findings
275 imply that the non-lethal caspase activation driven by *Fas3G* overexpression is orchestrated by
276 an increase in Dronc induced by Fas3G, bringing Dronc in close vicinity to Fas3G and thus
277 enabling caspase activation near the cell membrane (Fig. 5F).
278
279 ***Non-lethal caspase activation regulates innate attraction behavior***
280 Finally, we examined the function of *Fas3G* overexpression-facilitated non-lethal caspase
281 activation. Apple cider vinegar (ACV) excites six glomeruli in the AL, including DM1, which
282 is innervated by the axons of Or42b neurons [26]. We have previously reported that Or42b
283 neurons undergo aging-dependent caspase activation, which reduces neural activity and
284 attraction behavior in response to ACV [22]. Inhibition of caspase activity in aged flies restores
285 attraction behavior but does not affect that of young flies [22]. Using a two-choice preference
286 assay with ACV (Fig. 6A), we found that the overexpression of *Fas3G*, which activates
287 caspases, did not impair attraction behavior in young flies (Fig. 6B, C). In contrast,
288 simultaneous inhibition of *Fas3G* overexpression-facilitated non-lethal caspase activation
289 promoted attraction to ACV (Fig. 6B, C). Overall, these results suggest that *Fas3G*
290 overexpression-facilitated non-lethal caspase activation suppresses innate attractive behavior
291 without killing the cells.

292 **Discussion**

293 ***Proximal proteins of executioner caspases regulate non-lethal caspase activity***

294 It is important to identify the proximal proteins of executioner caspases, which cleave a wide
295 range of substrates and are essential for apoptosis [11,12], as proximity often dictates substrate
296 specificity [17]. In humans, Caspase-3 and Caspase-7 have been shown to share but also have
297 discrete substrate preferences [27]. Caspase-7 leverages an exosite to facilitate interaction with
298 RNA and enhance the proteolysis of RNA-binding proteins [28,29]. Thus, protein proximity
299 can be used to precisely regulate specific cellular functions by selectively cleaving a limited
300 pool of substrates in non-lethal scenarios compared with lethal cleavages where all the
301 substrates are potentially cleaved during apoptosis. Our current investigation showed that
302 executioner caspases, before activation as proforms, are exclusively sequestered in specific
303 subcellular domains, including the plasma membrane. We found that *Fas3G* overexpression
304 facilitates non-lethal activation, underscoring the importance of protein proximity not only in
305 substrate cleavage, but also in localizing non-lethal activation to the vicinity of plasma
306 membrane (Fig. 5F).

307

308 ***MASCaT as a highly sensitive reporter for identifying non-lethal caspase regulators***

309 Various caspase activity reporters have been developed, including SCAT3, a FRET-based
310 reporter with superior temporal resolution [30], CaspaseTracker/CasExpress, Caspase-
311 activatable Gal4-based reporters with superior sensitivity [20,21]. However, to date, no reporter
312 has been developed that is sensitive enough to identify non-lethal regulators of caspases in cells
313 of interest. In this study, we developed a novel caspase reporter, MASCaT, that can detect non-
314 lethal caspase activation with high sensitivity in a cell type-specific manner following gene
315 manipulation. Using MASCaT, we identified previously overlooked regulators of non-lethal
316 activation of caspases in a cell type-specific manner. Proximal proteins of executioner caspases

317 are potential non-lethal regulators, and combining TurboID-mediated identification of these
318 proteins will pave the way for identifying non-lethal components and broaden our
319 understanding of the molecular mechanism of non-lethal caspase activation.
320
321 ***Non-lethal caspase activation regulates neural activity and behaviors***
322 We previously reported that age-dependent caspase activation reduces neural activity and innate
323 attraction behavior [22]. Here, we found that, while *Fas3G* overexpression did not impair
324 attraction behavior by itself, caspase activation upon *Fas3G* overexpression suppressed
325 attraction behavior toward ACV (Fig. 6A, B). In mice, L1CAM, an immunoglobulin-like cell
326 adhesion molecule, facilitates neuronal excitability by regulating the voltage-gated Na+
327 channels [31]. Thus, we hypothesize that non-lethal caspase activation antagonizes the neuronal
328 excitability promoted by Fas3G. In neurons, caspases have diverse non-lethal functions,
329 including axon degeneration and macro- and micro-pruning, to regulate synaptic plasticity
330 [32,33]. In presynaptic terminals, it has been recently reported that Caspase-3 modulates
331 synaptic vesicle pools via autophagy [34]. Thus, it is possible that non-lethal activation
332 regulates synaptic pools and neural activity in a reversible manner without killing the cells.
333 Analyzing the functions mediated by Drice and Fas3G proximity, including the identification
334 of specific substrates, will pave the way for identifying diverse CDPs and understanding their
335 molecular mechanisms.
336 While suppressing innate attraction behavior does not seem beneficial by itself, it should
337 be a great advantage in decision-making. To survive, flies must constantly make appropriate
338 behavioral decisions (e.g., feeding versus mating) depending on their physiological conditions.
339 In males, a subset of neurons regulated by tyramine controls feeding versus mating behaviors
340 [35]. In regard of that, it is important to adequately promote or suppress neural activity, which

341 controls behaviors of the organisms, by precisely controlling caspase activation in a
342 subcellularly restricted manner in neurons.
343
344 ***Proximal proteins of executioner caspases define the site of caspase activation "hotspot"***
345 Although the core apoptotic machinery has been well characterized during the last 30 years [2],
346 the precise regulation of CDPs, remains incompletely elucidated. In this study, we identified
347 *Fas3G* overexpression activates Drice. Mechanistically, we found that *Fas3G* overexpression
348 induced the expression of initiator caspase Dronc, which also comes close to Fas3G, regulating
349 non-lethal caspase activation. Direct overexpression of Dronc alone results in cell death within
350 olfactory receptor neurons (Fig. 4A, B). However, when Dronc expression is upregulated due
351 to *Fas3G* overexpression, it does not lead to cell death in ORNs (Fig. 4C, D). The exact process
352 by which Dronc expression is increased in response to *Fas3G* overexpression remains to be
353 elucidated. It is known that Dronc can be upregulated via the ecdysone signaling pathway [36]
354 and the Hippo signaling pathway [37]. Therefore, the overexpression of *Fas3G* might
355 potentially activate Dronc expression through one or both of these signaling pathways. Fas3 is
356 an immunoglobulin-like domain-containing transmembrane protein that regulates axonal
357 fasciculation and neuronal projections [18]. NCAM, a mammalian homologue of Fascicilin 2,
358 is an immunoglobulin-like domain-containing cell adhesion molecule. NCAM can physically
359 bind to Caspase-8, and depending on NCAM clustering, Caspase-8 and -3 are activated and
360 contribute to neurite outgrowth by cleaving its substrate spectrin [38]. Thus, it seems likely that
361 cell adhesion molecule-mediated subcellularly restricted caspase activation is conserved among
362 species. Indeed, caspase-9/Apaf-1-dependent caspase-3 activation, without resulting in cell
363 death, has also been observed in the axon of olfactory sensory neurons during mouse
364 development [3]. A critical insight from our research is that the executioner caspase is pre-
365 compartmentalized in proximity to a specific set of proteins prior to activation, poised for the

366 initiator caspase to approach. Consequently, the "hotspot" for non-lethal caspase activity
367 appears to be determined by these neighboring proteins. While the "hotspot" located in the axon
368 of the ORN may exert an inhibitory effect on neural activity, it could also play a role in avoiding
369 cell death by localizing caspase activity, especially during development.

370 Recently, a protein interactome analysis in humans showed that tissue-preferentially
371 expressed proteins that interact with known apoptosis regulators participate in apoptosis
372 sensitization [39]. Given that CDPs are often cell-and tissue type-specific processes, the
373 identification of modulators of context-dependent apoptotic pathways will aid in understanding
374 the precise molecular regulation of CDPs. Importantly, alternative splicing can diversify
375 protein-protein interaction networks. A recent report showed that minor spliceosomes regulate
376 alternative splicing, including Fas3. A specific isoform of Fas3 has distinct functions and cannot
377 be substituted by other isoforms during neuronal development [40]. Our results support the idea
378 that alternative splicing may not only diversify the protein itself, but also its interaction
379 networks to regulate module-dependent activation. Further interactome analysis using TurboID
380 will reveal the regulatory mechanisms of the non-lethal activation of caspases.

381 **Materials and Methods**

382 ***Fly strains and rearing conditions***

383 We raised the flies in standard *Drosophila* medium at 25°C. For in vivo biotin labeling
384 experiments, flies were raised in standard *Drosophila* medium supplemented with 100 μM (+)-
385 biotin (#132-02635, WAKO). The following fly strains were used in this study: w^{1118},
386 *Drice::V5::TurboID*, *Dcp-1::V5::TurboID*, *Dronc::V5::TurboID* [16], *Pebbled-Gal4*
387 (BL80570), *LN-Gal4* (BL63325), *GH146-Gal4* (BL30026), *UAS-Drice-RNAi* (V28065),
388 *Fas3::EGFP::FlAsH::StrepII::TEV::3xFLAG* (BL59809), *UASz-Fas3A::3xFLAG*, *UASz-*
389 *Fas3B::3xFLAG*, *UASz-Fas3C::3xFLAG*, *UASz-Fas3D::3xFLAG*, *UASz-Fas3G::3xFLAG*
390 (this study), *Ubi-FRT-STOP-FRT-mCD8::DQVD::QF2*, *Ubi-FRT-STOP-FRT-*
391 *mCD8::DQVA::QF2* (this study), *UAS-FLP* (K107788), *QUAS-tdTomato::3xHA* (BL30005),
392 *ELAV-Gal4* (BL8765), *Or42b-Gal4* (BL9971), *UAS-RedStinger* (BL8547), *UASz-*
393 *myc::mNeonGreen*, *UASz-Drice::myc::mNeonGreen* (this study), *UASz-V5::TurboID*, *UASz-*
394 *Drice::V5::TurboID*, *UASz-Drice*^{CG}*::V5::TurboID*, *UASz-Dcp-1::V5::TurboID*, *UASz-Dcp-*
395 *1*^{CG}*::V5::TurboID*, *UASz-Dronc::V5::TurboID*, *UASz-Dronc*^{CG}*::V5::TurboID* (this study),
396 *UAS-Diap-1::VENUS* [41], *UAS-Dronc-RNAi* [9], *UAS-Dronc*^{DN} (a gift from H. Richardson),
397 *UAS-LacZ-RNAi*, *UAS-Fas3-RNAi#1* (V940), *UAS-Fas3-RNAi#2* (V3091), *UAS-Fas3G-RNAi*
398 (this study). BL, Bloomington Drosophila Resource Center; K, Kyoto Stock Center; V, Vienna
399 Drosophila Resource Center.

400

401 ***Detailed genotypes***

402 Fig. 1B, C (Left to Right, Top to Bottom)

403 w^{1118}*/Y*

404 *w/Y; Dcp-1::V5::TurboID/+*

405 *w/Y;; Drice::V5::TurboID/+*

406 *w/Y;; Dronc::V5::TurboID/+*

407

408 Fig. 1D (Left to Right)

409 *w; UAS-Drice-RNAi/+; Drice::V5::TurboID/+*

410 *w, Pebbled-Gal4/w; UAS-Drice-RNAi/+; Drice::V5::TurboID/+*

411 *w; UAS-Drice-RNAi/GH146-Gal4; Drice::V5::TurboID/+*

412 *w; UAS-Drice-RNAi/+; Drice::V5::TurboID/LN-Gal4*

413

414 Fig. 1E (Left to Right)

415 w^{1118}/Y

416 *w/Y;; Drice::V5::TurboID/+*

417

418 Fig. 1G (Left to Right)

419 w^{1118}/Y

420 *w/Y;; Drice::V5::TurboID/+*

421

422 Fig. 2A (Left to Right)

423 w^{1118}/Y

424 *w/Y;; Drice::V5::TurboID/+*

425

426 Fig. 2B (Top to Bottom, Left to Right)

427 w^{1118}/Y

428 *w/Y;; Drice::V5::TurboID/+*

429 *w/Y; Fas3::EGFP::FlAsH::StrepII::TEV::3xFLAG/+*

430 *w/Y; Fas3:: EGFP::FlAsH::StrepII::TEV::3xFLAG/+; Drice::V5::TurboID/+*

431

432 Fig. 2E (Left to Right)

433 *w, Pebbled-Gal4/w or Y*

434 *w, Pebbled-Gal4/w or Y;; UASz-Fas3A::3xFLAG/+*

435 *w, Pebbled-Gal4/w or Y;; UASz-Fas3B::3xFLAG/+*

436 *w, Pebbled-Gal4/w or Y;; UASz-Fas3C::3xFLAG/+*

437 *w, Pebbled-Gal4/w or Y;; UASz-Fas3D::3xFLAG/+*

438 *w, Pebbled-Gal4/w or Y;; UASz-Fas3G::3xFLAG/+*

439

440 Fig. 2F (Left to Right)

441 w^{1118}/Y

442 *w/Y;; Drice::V5::TurboID/+*

443

444 Fig. 2G (Left to Right)

445 *w, Pebbled-Gal4/w or Y;; Drice::V5::TurboID/+*

446 *w, Pebbled-Gal4/w or Y;; Drice::V5::TurboID/UASz-Fas3A::3xFLAG*

447 *w, Pebbled-Gal4/w or Y;; Drice::V5::TurboID/UASz-Fas3B::3xFLAG*

448 *w, Pebbled-Gal4/w or Y;; Drice::V5::TurboID/UASz-Fas3C::3xFLAG*

449 *w, Pebbled-Gal4/w or Y;; Drice::V5::TurboID/UASz-Fas3D::3xFLAG*

450 *w, Pebbled-Gal4/w or Y;; Drice::V5::TurboID/UASz-Fas3G::3xFLAG*

451

452 Fig. 3C (Top to Bottom)

453 *w/Y; Ubi-FRT-STOP-FRT-mCD8::DQVD::QF2/+; UAS-FLP, QUAS-tdTomato::3xHA/+*

454 *w/Y; Ubi-FRT-STOP-FRT-mCD8::DQVA::QF2/ELAV-Gal4; UAS-FLP, QUAS-*

455 *tdTomato::3xHA/+*

456 *w/Y; Ubi-FRT-STOP-FRT-mCD8::DQVD::QF2/ELAV-Gal4; UAS-FLP, QUAS-*
457 *tdTomato::3xHA/+*
458
459 Fig. 4A, B (Top to Bottom, Left to Right)
460 *w/Y; Or42b-Gal4/+; UAS-RedStinger/UASz-V5::TurboID*
461 *w/Y; Or42b-Gal4/+; UAS-RedStinger/UASz-Drice^{CG}::V5::TurboID*
462 *w/Y; Or42b-Gal4/+; UAS-RedStinger/UASz-Drice::V5::TurboID*
463 *w/Y; Or42b-Gal4/+; UAS-RedStinger/UASz-Dcp-1^{CG}::V5::TurboID*
464 *w/Y; Or42b-Gal4/+; UAS-RedStinger/UASz-Dcp-1::V5::TurboID*
465 *w/Y; Or42b-Gal4/+; UAS-RedStinger/UASz-Dronc^{CG}::V5::TurboID*
466 *w/Y; Or42b-Gal4/+; UAS-RedStinger/UASz-Dronc::V5::TurboID*
467
468 Fig. 4C, D (Top to Bottom, Left to Right)
469 *w/Y; Or42b-Gal4/UASz-3xFLAG::mNeonGreen; UAS-RedStinger/+*
470 *w/Y; Or42b-Gal4/+; UAS-RedStinger/UASz-Fas3G::3xFLAG*
471 *w/Y; Or42b-Gal4/UASz-Drice::myc::mNeonGreen; UAS-RedStinger/+*
472 *w/Y; Or42b-Gal4/UASz-Drice::myc::mNeonGreen; UAS-RedStinger/UASz-Fas3G::3xFLAG*
473
474 Fig. 4E (Top to Bottom)
475 *w/Y; Or42b-Gal4/UASz-3xFLAG::mNeonGreen*
476 *w/Y; Or42b-Gal4, Ubi-FRT-STOP-FRT-mCD8::DQVD::QF2/UASz-3xFLAG::mNeonGreen;*
477 *UAS-FLP, QUAS-tdTomato::3xHA/+*
478
479 Fig. 4F, G (Top to Bottom, Left to Right)

480 *w/w or Y; Or42b-Gal4, Ubi-FRT-STOP-FRT-mCD8::DQVD::QF2/UASz-*
481 *3xFLAG::mNeonGreen; UAS-FLP, QUAS-tdTomato::3xHA/+*
482 *w/w or Y; Or42b-Gal4, Ubi-FRT-STOP-FRT-mCD8::DQVD::QF2/+; UAS-FLP, QUAS-*
483 *tdTomato::3xHA/UASz-Fas3G::3xFLAG*
484 *w/w or Y; Or42b-Gal4, Ubi-FRT-STOP-FRT-mCD8::DQVD::QF2/UASz-*
485 *Drice::myc::mNeonGreen; UAS-FLP, QUAS-tdTomato::3xHA/+*
486 *w/w or Y; Or42b-Gal4, Ubi-FRT-STOP-FRT-mCD8::DQVD::QF2/UASz-*
487 *Drice::myc::mNeonGreen; UAS-FLP, QUAS-tdTomato::3xHA/UASz-Fas3G::3xFLAG*
488
489 Fig. 4H, I (Top to Bottom, Left to Right)
490 *w/w or Y; Or42b-Gal4, Ubi-FRT-STOP-FRT-mCD8::DQVD::QF2/UASz-*
491 *3xFLAG::mNeonGreen; UAS-FLP, QUAS-tdTomato::3xHA/+*
492 *w/w or Y; Or42b-Gal4, Ubi-FRT-STOP-FRT-mCD8::DQVD::QF2/+; UAS-FLP, QUAS-*
493 *tdTomato::3xHA/UASz-Fas3G::3xFLAG*
494 *w/w or Y; Or42b-Gal4, Ubi-FRT-STOP-FRT-mCD8::DQVD::QF2/UAS-Diap-1::VENUS;*
495 *UAS-FLP, QUAS-tdTomato::3xHA/UASz-Fas3G::3xFLAG*
496
497 Fig. 5A (Left to Right)
498 *w, Pebbled-Gal4/Y*
499 *w, Pebbled-Gal4/Y;; Dronc::V5::TurboID/+*
500 *w, Pebbled-Gal4/Y;; Dronc::V5::TurboID/UASz-Fas3G::3xFLAG*
501
502 Fig. 5B (Left to Right)
503 *w, Pebbled-Gal4/Y;; Dronc::V5::TurboID/+*
504 *w, Pebbled-Gal4/Y;; Dronc::V5::TurboID/UASz-Fas3G::3xFLAG*

w, Pebbled-Gal4/Y;; Dronc::V5::TurboID/UASz-Fas3C::3xFLAG

Fig. 5C, D (Top to Bottom, Left to Right)

w/w or Y; Or42b-Gal4, Ubi-FRT-STOP-FRT-mCD8::DQVD::QF2/UASz-3xFLAG::mNeonGreen; UAS-FLP, QUAS-tdTomato::3xHA/+

w/w or Y; Or42b-Gal4, Ubi-FRT-STOP-FRT-mCD8::DQVD::QF2/+; UAS-FLP, QUAS-tdTomato::3xHA/UASz-Fas3G::3xFLAG

w/w or Y; Or42b-Gal4, Ubi-FRT-STOP-FRT-mCD8::DQVD::QF2/UAS-Dronc-RNAi; UAS-FLP, QUAS-tdTomato::3xHA/UASz-Fas3G::3xFLAG

w/w or Y; Or42b-Gal4, Ubi-FRT-STOP-FRT-mCD8::DQVD::QF2/UAS-Dronc^{DN}; UAS-FLP, QUAS-tdTomato::3xHA/UASz-Fas3G::3xFLAG

Fig. 5E (Left to Right)

w, Pebbled-Gal4/Y;; Drice::V5::TurboID/+

w, Pebbled-Gal4/Y;; Drice::V5::TurboID/UASz-Fas3G::3xFLAG

w, Pebbled-Gal4/Y; +/UAS-Dronc-RNAi; Drice::V5::TurboID/UASz-Fas3G::3xFLAG

w, Pebbled-Gal4/Y; +/UAS-Dronc^{DN}; Drice::V5::TurboID/UASz-Fas3G::3xFLAG

Fig. 6B, C (Left to Right)

w/Y; Or42b-Gal4/UASz-3xFLAG::mNeonGreen

w/Y; Or42b-Gal4/+; +/UASz-Fas3G::3xFLAG

w/Y; Or42b-Gal4/UAS-Dronc-RNAi; +/UASz-Fas3G::3xFLAG

w/Y; Or42b-Gal4/UAS-Dronc^{DN}; +UASz-Fas3G::3xFLAG

Fig. S1A (Left to Right, Top to Bottom)

530 *w^{1118}/Y*

531 *w^{1118}*

532 *w/Y;; Drice::V5::TurboID/+*

533 *w/w^{1118};; Drice::V5::TurboID/+*

534

535 Fig. S2A (Left to Right)

536 *w, Pebbled-Gal4/w or Y;; Drice::V5::TurboID/+*

537 *w, Pebbled-Gal4/w or Y;; Drice::V5::TurboID/UASz-Fas3C::3xFLAG*

538 *w, Pebbled-Gal4/w or Y;; Drice::V5::TurboID/UASz-Fas3G::3xFLAG*

539

540 Fig. S4C, D (Top to Bottom, Left to Right)

541 *w/w or Y; Or42b-Gal4, Ubi-FRT-STOP-FRT-mCD8::DQVD::QF2/UAS-LacZ-RNAi; UAS-*

542 *FLP, QUAS-tdTomato::3xHA/+*

543 *w/w or Y; Or42b-Gal4, Ubi-FRT-STOP-FRT-mCD8::DQVD::QF2/+; UAS-FLP, QUAS-*

544 *tdTomato::3xHA/UAS-Fas3-RNAi #1*

545 *w/w or Y; Or42b-Gal4, Ubi-FRT-STOP-FRT-mCD8::DQVD::QF2/+; UAS-FLP, QUAS-*

546 *tdTomato::3xHA/UAS-Fas3-RNAi #2*

547 *w/w or Y; Or42b-Gal4, Ubi-FRT-STOP-FRT-mCD8::DQVD::QF2/UAS-Fas3G-RNAi; UAS-*

548 *FLP, QUAS-tdTomato::3xHA/+*

549

550 Fig. S4E (Left to Right, Top to Bottom)

551 *w, Pebbled-Gal4/Y; UASz-Drice::myc::mNeonGreen/+*

552 *w, Pebbled-Gal4/Y; UASz-Drice::myc::mNeonGreen/+; UASz-Fas3G::3xFLAG/+*

553 *w, Pebbled-Gal4/Y; UASz-Drice::myc::mNeonGreen/+; UAS-Fas3-RNAi #1/+*

554 *w, Pebbled-Gal4/Y; UASz-Drice::myc::mNeonGreen/+; UAS-Fas3-RNAi #2/+*

555 *w, Pebbled-Gal4/Y; UASz-Drice::myc::mNeonGreen/UAS-Fas3G-RNAi*

556

557 ***Protein preparation from Drosophila tissues***

558 Adult heads or brains of the given genotype were dissected and lysed with RIPA buffer (50 mM
559 Tris-HCl, pH 8.0, 150 mM Sodium Chloride, 0.5 w/v% Sodium Deoxycholate, 0.1% w/v
560 Sodium Dodecyl Sulfate, and 1.0% w/v NP-40) supplemented with cOmplete ULTRA EDTA-
561 free protease inhibitor cocktail (#05892953001, Roche). Samples were homogenized and
562 centrifuged at 20,000 ×g, 4°C for 10 min. The supernatants were collected and snap-frozen in
563 liquid nitrogen. Protein concentrations were determined using the BCA assay (#297-73101,
564 Wako) following the manufacturer's protocol. The samples were mixed with 6x Laemmli
565 buffer, boiled at 95°C for 5 min, and then subjected to purification of biotinylated proteins and
566 western blot analysis.

567

568 ***Western blotting***

569 Each sample was separated using SDS-PAGE. The proteins were then transferred onto
570 Immobilon-P PVDF membranes (#IPVH00010; Millipore) for immunoblotting. Membranes
571 were blocked with 4% skim milk diluted in 1× TBST. Immunoblotting was performed using
572 the antibodies mentioned below diluted in 4% skim milk. Signals were visualized using
573 Immobilon Western Chemiluminescent HRP Substrate (#WBKLS0500; Millipore) and
574 FUSION SOLO. 7S. EDGE imaging station (Vilber-Lourmat). Contrast and brightness
575 adjustments were applied equally using Fiji (ImageJ) software (NIH Image).

576 The primary antibodies used included mouse anti-V5 monoclonal antibody (1:5,000,
577 #46-0705, Invitrogen), mouse anti-FLAG M2 monoclonal antibody (1:5,000, Sigma), mouse
578 anti-alpha tubulin (DM1A) monoclonal antibody (1:10,000, #T9026, Sigma), mouse anti-Actin
579 monoclonal antibody (1:5,000; #A4700, Sigma), mouse anti-Fasciclin 3 (7G10) antibody (1:50,

580 #AB_528238, DSHB), rabbit anti-Fasciclin3 isoform G antibody (1:50, this study), mouse anti-
581 Drosophila Lamin B monoclonal antibody (1:1000, #ADL67.10, DSHB). The secondary
582 antibodies used included goat anti-rabbit IgG HRP-conjugated antibody (1:5,000, #7074S,
583 CST) and goat/rabbit/donkey anti-mouse IgG HRP Conjugate (1:5,000, #W402B, Promega).
584 The membranes for streptavidin blotting were blocked with 3% BSA. Streptavidin blotting was
585 performed using streptavidin-horseradish peroxidase (1:10,000, #SA10001; Invitrogen) diluted
586 in 3% BSA.
587
588 ***Co-immunoprecipitation***
589 Adult heads were lysed on ice using DDM IP lysis buffer (50 mM Tris-HCl (pH 7.5), 150 mM
590 NaCl, 0.2% N-Dodecyl-β-D-maltoside (DDM) (#341-06161, WAKO)) containing cOmplete
591 ULTRA EDTA-free protease inhibitor cocktail. The samples were adjusted to 150 μg
592 protein/150 μL DDM IP lysis buffer. The samples were incubated overnight at 4 °C with 10
593 μL anti-FLAG M2 Magnetic Beads (#M8823-1ML, Millipore) equilibrated with the DDM IP
594 lysis buffer. The beads were washed three times in wash buffer (50 mM Tris-HCl (pH 7.5),
595 150 mM NaCl, 0.1% DDM) and boiled for 5 min at 95 °C with 50 μL 1× Laemmli buffer. The
596 samples were magnetically separated, and the supernatants were subjected to SDS-PAGE.
597
598 ***Immunohistochemistry***
599 Adult brains were dissected in phosphate-buffered saline (PBS) and fixed in 4%
600 paraformaldehyde (PFA) at room temperature for 30 min. Adult brains were washed three times
601 with 0.3% PBST (Triton-X100) for 10 min. After blocking with 5.0% normal donkey serum
602 (#S30, Millipore)/PBST (PBSTn) for 30 minutes at room temperature, tissues were incubated
603 with primary antibody/PBSTn overnight at 4°C. The samples were then washed with PBST
604 three times for 10 min each and incubated with secondary antibody/PBSTn for 2 h at room

605 temperature. After incubation, the tissues were washed with PBST three times for 10 min.
606 Streptavidin and Hoechst 33342 were added during secondary antibody incubation. The
607 samples were mounted on glass slides with SlowFade Gold antifade reagent (#S36939,
608 Invitrogen). Images were captured using a Leica TCS SP8 micrscope (Leica Microsystems).
609 Images were analyzed and edited using the Fiji (ImageJ) software. For MASCaT analysis,
610 newly eclosed adults were raised at 29°C for 1 week. Classification of the MASCaT signal was
611 performed by optically assessing the tdTomato intensity. For cell number analysis, newly
612 eclosed adults were raised at 29°C for 1 week. The antennae were dissected as previously
613 described [42], fixed with 4% PFA at room temperature for 30 min, and washed with 0.4%
614 PBST (Triton-X100) three times for 10 min. Quantification of cell numbers in antenna was
615 performed using Fiji (ImageJ) software using "3D object counter" for RedStinger positive cells.
616 The primary antibodies used were mouse anti-Fasciclin 3 (7G10) antibody (1:20,
617 #AB_528238, DSHB), rat anti-GFP (GF090R) monoclonal antibody (1:100, #04404-26,
618 nacalai Tesque), mouse anti-FLAG M2 monoclonal antibody (1:500, F1804, Sigma), and rat
619 anti-mCD8 monoclonal antibody (1:50, #MCD0800, Invitrogen). The secondary antibodies
620 used included Alexa Fluor 488-conjugated donkey anti-mouse IgG antibody (1:500, #A-21202,
621 ThermoFisher Scientific), Alexa Fluor 488-conjugated donkey anti-rat IgG antibody (1:500,
622 #A-21208, ThermoFisher Scientific), Alexa Fluor 647-conjugated donkey anti-mouse IgG
623 antibody (1:500, #A-31571, ThermoFisher Scientific), and Alexa Fluor 633-conjugated goat
624 anti-rat IgG antibody (1:500, #A-21094, ThermoFisher Scientific). The nuclei were stained
625 with Hoechst 33342 (8 μM, #H3570, Invitrogen). Streptavidin-Cy2 (1:500, #016-220-084,
626 Jackson ImmunoResearch) and Streptavidin-Cy5 (1:500, #016-170-084, Jackson
627 ImmunoResearch) were used to stain the biotinylated proteins.
628
629 ***Experimental design for LC-MS/MS analyses***

630 Two biological replicates were analyzed for each experimental condition to determine the
631 relative abundance of *Drice::V5::TurboID/w*^{1118}.
632
633 ***Purification of biotinylated proteins***
634 Samples were prepared as previously described [17]. Briefly, 100 µg of biotinylated protein-
635 containing lysate (from 100 brains or 20 heads) was subjected to FG-NeutrAvidin bead
636 (#TAS8848 N1171, Tamagawa Seiki) purification. The FG-NeutrAvidin beads (25 µL,
637 approximately 500 µg) were washed three times with RIPA buffer. Benzonase-treated
638 biotinylated protein samples suspended in 1 mL RIPA buffer were incubated overnight at 4°C.
639 Conjugated beads were magnetically isolated and washed with 500 µL of an ice-cold RIPA
640 buffer solution, 1 M KCl solution, 0.1 M Na_2CO_3 solution and 4 M urea solution. For western
641 blot analyses, the purified samples were mixed with Laemmli buffer, boiled at 95°C for 5 min,
642 and then subjected to western blot analysis. For LC-MS/MS analysis, the purified samples were
643 washed with 500 µL ultrapure water (#214-01301, Wako) and 500 µL of 50 mM ammonium
644 bicarbonate (AMBC). The samples were then mixed with 50 µL of 0.1% Rapigest diluted in 50
645 mM AMBC, and 5 µL of 50 mM TCEP was subsequently added. Samples were incubated at
646 60°C for 5 min, and then 2.5 µL 200 mM MMTS was added. One microgram sequence-grade
647 modified trypsin (#V5111, Promega) was then added for on-bead trypsin digestion at 37°C for
648 16 h. The beads were magnetically isolated and 60 µL of the supernatant was collected. Then,
649 3 µL 10% TFA was added to the supernatants, and the samples were incubated at 37°C for 60
650 min with gentle agitation. The samples were then centrifuged at 20,000 ×g, 4°C for 10 min. The
651 peptides were desalinated and purified using a GL-tip SDB (#7820-11200, GL Sciences)
652 following the manufacturer's protocol. The samples were speed-backed at 45°C for 30 min and
653 dissolved in 25 µL of 0.1% formic acid. The samples were then centrifuged at 20,000 ×g, 4°C
654 for 10 min, and the supernatants were collected. The peptide concentrations were determined

655 using the BCA assay. Finally, 500 ng of the purified protein was subjected to LC-MS/MS
656 analysis.
657
658 ***LC-MS/MS analyses***
659 LC-MS/MS analyses were performed as previously described [17]. Briefly, samples were
660 loaded onto Acclaim PepMap 100 C18 column (75 µm x 2 cm, 3 µm particle size and 100 Å
661 pore size; #164946, ThermoFisher Scientific) and separated on nano-capillary C18 column, (75
662 µm x 12.5 cm, 3 µm particle size, #NTCC-360/75-3-125, Nikkyo Technos) using EASY-nLC
663 1200 system (ThermoFisher Scientific). The elution conditions are listed in Table S3. The
664 separated peptides were analyzed using QExactive (ThermoFisher Scientific) in data-dependent
665 MS/MS mode. The parameters for the MS/MS analysis are listed in Table S4. The collected
666 data were analyzed using Proteome Discoverer (PD) 2.2 software with the Sequest HT search
667 engine. The parameters for the PD 2.2 analysis are described in Table S5. Peptides were filtered
668 at a false discovery rate of 0.01 using the Percolator node. Label-free quantification was
669 performed based on the intensities of the precursor ions using a precursor-ion quantifier node.
670 Normalization was performed using the total amount of peptides in all average scaling modes.
671 Proteins with 10 folds or higher abundance relative to the control (w^{1118}) were considered for
672 further analysis. MS proteomic data were deposited in the ProteomeXchange Consortium via
673 the jPOST partner repository with the dataset identifier PXD042922 [43].
674
675 ***Gene Ontology analysis***
676 Gene Ontology (GO) analysis of cellular components was performed using DAVID [44].
677
678 ***Generation of rabbit polyclonal anti-Fasciclin 3 isoform G antibody***

679 The peptide corresponding to the 506–524 AA (N-LKPANEATPATTPAPTTAA-C) of Fas3G
680 was used by Eurofins Inc. to immunize rabbits to raise a polyclonal antibody. The antibody was
681 affinity purified using the same peptide provided by Eurofins, Inc.
682
683 ***IDR prediction***
684 Amino acid sequences were obtained from the FlyBase database [https://flybase.org/].
685 Disordered intracellular regions of Fas3 isoforms were predicted using the PSIPRED protein
686 sequence analysis workbench in DISOPRED3 [http://bioinf.cs.ucl.ac.uk/psipred/].
687
688 ***Molecular cloning***
689 For all isoforms (A, B/F, C, D/E, G) of *pUASz-Fasciclin 3::3xFLAG*, the coding sequences of
690 Fasciclin 3s were PCR-amplified using 3xFLAG-tag harboring primers from *Drosophila* cDNA
691 and were ligated into the *BamH*I/*Kpn*I-digested *pUASz1.0* vector [45] using In-Fusion
692 (#Z9648N, TaKaRa). For all isoforms of *pAc5-Fasciclin 3::3xFLAG*, the coding sequence of
693 *Fasciclin 3s::3xFLAG* were PCR-amplified from corresponding *pUASz-Fasciclin 3::3xFLAG*
694 vectors and were ligated into the *EcoR*I/*Xho*I-digested *pAc5-STABLE2-neo* vector using
695 NEBuider HiFi DNA Assembly. using NEBuilder HiFi DNA Assembly (#E2621L, NEB). For
696 *pUASz-3xFLAG::mNeonGreen*, the coding sequence of mNeonGreen was PCR-amplified
697 using 3xFLAG-tag harboring primers from *pAc5-V5::mNeonGreen* [17] and ligated into the
698 *Xho*I-digested *pUASz1.0* vector [45] using In-Fusion. For *pUASz-Drice::myc::mNeonGreen*,
699 the coding sequence of mNeonGreen was PCR-amplified from *pAc5-V5::mNeonGreen* [17]
700 using myc-tag-harboring primers. The coding sequence of Drice was PCR-amplified from
701 *Drosophila* cDNA. The two fragments were then ligated into the *Xho*I-digested *pUASz1.0*
702 vector using In-Fusion. For *pUASz-V5::TurboID* and *pUASz-Caspase::V5::TurboID*, the
703 coding sequences of *Dcp-1*, *Drice* and *Dronc* were PCR amplified from *Drosophila* cDNA.

704 The coding sequence of V5::TurboID was PCR-amplified from *V5-TurboID-NES_pcDNA3*
705 (#107169; Addgene). The two fragments were then ligated into the *Xho*I-digested *pUASz1.0*
706 vector using In-Fusion. Catalytic dead mutations (Dcp-1: C196G (TGC to GGC), Drice: C211G
707 (TGC to GGC), and Dronc: C318G (TGC to GGC)) were introduced by PCR-based site-
708 directed mutagenesis, and the corresponding fragments were ligated into the *Xho*I-digested
709 *pUASz1.0* vector using In-Fusion. For *pJFRC-mCD8::DQVD/A::QF2*, the coding sequence of
710 *mCD8::DQVD/A* were PCR-amplified from genomic DNA of *Caspase-Sensitive/Insensitive-*
711 *Gal4* [20]. The coding sequence of *QF2* was PCR-amplified from *pBPQU* vector [46]. These
712 fragments were ligated into the *Xho*I/*Xba*I-digested *pJFRC-28K* vector [45] using In-Fusion.
713 For *pUbi-FRT-STOP-FRT-mCD8::DQVD/A::QF2*, the FRT-STOP-FRT cassette sequence
714 was PCR amplified from *pJFRC201-10xUAS-FRT-STOP-FRT-myr::smGFP-HA* (#63166;
715 Addgene). The coding sequence of mCD8::DQVD/A was PCR-amplified from the genomic
716 DNA of *Caspase-Sensitive/Insensitive-Gal4* [20]. The coding sequence of QF2 was PCR
717 amplified from the *pBPQUw* plasmid [46]. The three fragments were ligated into *EcoR*I-
718 digested *pUbi83* vector (a gift from D. Umetsu) using In-Fusion. For *pQUAST-mNeonGreen*,
719 the coding sequence of mNeonGreen was PCR-amplified from *pAc5-V5::mNeonGreen* [17]
720 and ligated into the *EcoR*I-digested *pQUAST* (#24349, Addgene) vector using In-Fusion. For
721 *pUASz-FLPo*, the coding sequences of FLPo were PCR-amplified from *pQUAST-FLPo*
722 (#24357, Addgene) and ligated into the *Xho*I-digested *pUASz1.0* vector [45] using In-Fusion.
723 For *pWALIUM20-Fas3G-shRNA*, the top and bottom oligonucleotides including *mRNA*
724 sequence specific to isoform G (5'-AATGAACCAAAGCAAGACAAA-3') were annealed in
725 annealing buffer (10 mM Tris-HCl, 0.1 M NaCl, 1 mM EDTA). The annealed fragment was
726 ligated into *Nhe*I/*Eco*RI-digested *pWALIUM20* (#1472, DGRC) vector using DNA Ligation Kit
727 <Mighty Mix> (#6023, TaKaRa).

728 All established plasmids were sequenced by Eurofins, Inc. The detailed plasmid DNA
729 sequences are available upon request. The established plasmids were injected into y^1, w^{67c23};
730 *P[CaryP]attP40* (*pUASz-3xFLAG::mNeonGreen*, *pUASz-Drice::myc::mNeonGreen* and
731 *pWALIUM20-Fas3G-shRNA*) or y^1, w^{67c23}; *P[CaryP]attP2* (*pUASz-Fasciclin 3s::3xFLAG*,
732 *pUbi-FRT-STOP-FRT-mCD8::DQVD/A::QF2*, *pUASz-V5::TurboID* and *pUASz-*
733 *Caspase::V5::TurboID,*) for PhiC31-mediated transgenesis (BestGene Inc.). Each red-eye-
734 positive transformant was isogenized. Integration of the attP landing site was confirmed using
735 genomic PCR.
736
737 ***Cell culture***
738 *Drosophila* S2 cells were grown at 25°C in Schneider's *Drosophila* medium (#21720001,
739 GIBCO) supplemented with 10% (v/v) heat-inactivated fetal bovine serum, 100 U/ml penicillin,
740 and 100 μg/ml streptomycin (#168-23191, WAKO). Cells were seeded in 24-well plates and
741 transfected with the desired plasmids using Effectene Transfection Reagent (#301427,
742 QIAGEN) following the manufacturer's protocol. Sixteen hours after transfection, the cells
743 were reseeded into CELL CULTURE DISH, PS, 35/10 MM (#627870, Grainer BIO-ONE) and
744 incubated for 24 h. Images were obtained using a Leica AF6000 DMI6000 B microscope (Leica
745 Microsystems). Images were analyzed and edited using Fiji software (NIH Image).
746 For the substrate cleavage assay, cells were seeded in 12-well plates and were
747 transfected with desired *pAc5-Fas3::3xFLAG* plasmids using Effectene Transfection Reagent
748 following the manufacturer's protocol. After 40 h of incubation, the cells were treated with
749 10 μg/mL cycloheximide (CHX, #C7698, Sigma) for apoptosis induction. After 6 h of
750 incubation, cells were collected using RIPA buffer supplemented with cOmplete ULTRA
751 EDTA-free protease inhibitor cocktail depending on the cell status. For apoptotic cell lysate
752 collection, cells were resuspended by pipetting and were collected into a 1.5 mL tube. The cells

753 were then centrifuged at 800 g, 4 °C for 5 min, resuspended in PBS, and centrifuged again using
754 the same parameters. The cell pellets were then lysed with 100 μL RIPA buffer. For the other
755 experimental conditions, the cells were washed thrice with PBS and directly lysed on the plate
756 with 100 μL RIPA buffer. The supernatants were collected and snap-frozen in liquid nitrogen.
757 Protein concentrations were determined using the BCA assay following the manufacturer's
758 protocol. The samples were mixed with 6x Laemmli buffer, boiled at 95°C for 5 min, and then
759 subjected to western blot analysis.

760 For the validation of Fas3G-shRNA, cells were seeded in 12-well plates and were co-
761 transfected with *pActin-Gal4,* desired *pUASz-Fas3::3xFLAG* and *pWALIUM20-empty* or
762 *pWALIUM20-Fas3G-shRNA* plasmids using Effectene Transfection Reagent following the
763 manufacturer's protocol. After 40 h of incubation, the cells were washed thrice with PBS and
764 directly lysed on the plate with 100 μL RIPA buffer. The supernatants were collected and snap-
765 frozen in liquid nitrogen. Protein concentrations were determined using the BCA assay
766 following the manufacturer's protocol. The samples were mixed with 6x Laemmli buffer,
767 boiled at 95°C for 5 min, and then subjected to western blot analysis.

768

769 ***Aging experiment***

770 Adult male flies were raised in vials containing 15 fly/vial, and incubated at 29°C, 65%
771 humidity with 12h/12h light/dark cycle. The flies were transferred every 2–4 days to vials
772 containing fresh food.

773

774 ***Two choice preference assay***

775 Newly eclosed adult male flies were raised in vials containing 25 fly/vial, and incubated at 29°C,
776 65% humidity with 12h/12h light/dark cycle. The flies were transferred every 2–4 days to vials
777 containing fresh food for 1 week. The flies were starved in MilliQ (MQ) for 4 h prior to the

778 assay. About 75 flies were put in 1000-mL glass beaker, which contained two standards bottles
779 filled with 500 µl 1% ACV (Mizkan) and 500 µl MQ. The bottles were then covered with
780 sponge plugs containing pipette tips. The pipette tip was cut to increase the size of the opening
781 such that only one fly could climb into the bottle at a time. The glass beaker was covered with
782 a mesh fabric. The beakers were set in an incubator at 29°C for 2 hr for the assay. The
783 experiments were evaluated only if at least one of the tested flies entered either of 2 bottles.
784 The preference index equaled the number of flies in the ACV minus the number of flies in the
785 MQ, divided by the number of total live flies in both inside and outside of the bottles, and
786 multiplied by 100. Values greater than zero indicate a preference for 1% ACV and values less
787 than zero indicate aversion. We repeated the same experiment with different sets of flies and
788 the number of times is indicated by N.
789
790 ***Statistical analysis***
791 Statistical analyses were performed using the GraphPad Prism 8 software (MDF). Data are
792 shown as the means ± standard error of the mean. *P*-values were calculated using a one-way
793 analysis of variance (ANOVA) with Bonferroni correction (Fig. 4B for selected pairs, Fig. 4D
794 for every pair). *P*-values were calculated using the chi-square test with Bonferroni's correction,
795 with mNeonGreen as a control (Fig. 4G), LacZ-RNAi as a control (Fig. S4D), mNeonGreen
796 and Fas3G as controls (Fig. 4I, 5D), and mNeonGreen as a control (Fig. 6B). *P*-values were
797 calculated using one-way ANOVA with Dunnett's multiple comparison test (Fig. 6C,
798 mNeonGreen as a control). NS: $P > 0.05$, †: < 0.05.

Acknowledgments

We would like to thank Dr. D. Umetsu for providing plasmids, Dr. Y. Nitta, Dr. A. Sugie, and Dr. T. Ichinose for helpful discussions, and the Bloomington *Drosophila* Stock Center, Vienna Drosophila Resource Center and Kyoto Stock Center for providing the fly strains. We thank Dr. S. Hirayama, Dr. S. Murata, and the one-stop sharing faculty center for future drug discovery at the Graduate School of Pharmaceutical Sciences, University of Tokyo, for the LC-MS/MS analysis. We thank Miura's lab members for their technical assistance and discussions; in particular, K. Takenaga for preparing the fly food, and R. Takamoto for experimental support. The MASCaT was established by MASaya Muramoto with critical advice from members of Shu MASuda at MASayuki Miura Laboratories. We would like to thank *Editage* (www.editage.com) for English language editing of this manuscript.

810 **References**

811 1. Green DR. The Coming Decade of Cell Death Research: Five Riddles. Cell. 2019;177:
812 1094–1107. doi:10.1016/j.cell.2019.04.024
813 2. Nakajima YI, Kuranaga E. Caspase-dependent non-apoptotic processes in development.
814 Cell Death Differ. 2017;24: 1422–1430. doi:10.1038/cdd.2017.36
815 3. Ohsawa S, Hamada S, Kuida K, Yoshida H, Igaki T, Miura M. Maturation of the
816 olfactory sensory neurons by Apaf-1/caspase-9–mediated caspase activity. Proc Natl
817 Acad Sci U S A. 2010;107: 13366–13371. doi:10.1073/pnas.0910488107
818 4. Li Z, Jo J, Jia JM, Lo SC, Whitcomb DJ, Jiao S, et al. Caspase-3 activation via
819 mitochondria is required for long-term depression and AMPA receptor internalization.
820 Cell. 2010;141: 859–871. doi:10.1016/j.cell.2010.03.053
821 5. Aram L, Yacobi-Sharon K, Arama E. CDPs: Caspase-dependent non-lethal cellular
822 processes. Cell Death Differ. 2017;24: 1307–1310. doi:10.1038/cdd.2017.111
823 6. D'Brot A, Chen P, Vaishnav M, Yuan S, Akey CW, Abrams JM. Tango7 directs cellular
824 remodeling by the Drosophila apoptosome. Genes Dev. 2013;27: 1650–1655.
825 doi:10.1101/gad.219287.113
826 7. Kang Y, Neuman SD, Bashirullah A. Tango7 regulates cortical activity of caspases
827 during reaper-triggered changes in tissue elasticity. Nat Commun. 2017;8: 603.
828 doi:10.1038/s41467-017-00693-3
829 8. Orme MH, Liccardi G, Moderau N, Feltham R, Wicky-John S, Tenev T, et al. The
830 unconventional myosin CRINKLED and its mammalian orthologue MYO7A regulate
831 caspases in their signalling roles. Nat Commun. 2016;7: 10972.
832 doi:10.1038/ncomms10972

833 9. Kanuka H, Kuranaga E, Takemoto K, Hiratou T, Okano H, Miura M. Drosophila caspase
834 transduces Shaggy/GSK-3β kinase activity in neural precursor development. EMBO J.
835 2005;24: 3793–3806. doi:10.1038/sj.emboj.7600822
836 10. Amcheslavsky A, Wang S, Fogarty CE, Lindblad JL, Fan Y, Bergmann A. Plasma
837 Membrane Localization of Apoptotic Caspases for Non-apoptotic Functions. Dev Cell.
838 2018;45: 450-464.e3. doi:10.1016/j.devcel.2018.04.020
839 11. Julien O, Wells JA. Caspases and their substrates. Cell Death Differ. 2017;24: 1380–
840 1389. doi:10.1038/cdd.2017.44
841 12. Kumar S. Caspase function in programmed cell death. Cell Death Differ. 2007;14: 32–
842 43. doi:10.1038/sj.cdd.4402060
843 13. Kumar S, Dorstyn L, Lim Y. The role of caspases as executioners of apoptosis. Biochem
844 Soc Trans. 2022;50: 33–45. doi: 10.1042/BST20210751
845 14. Branon TC, Bosch JA, Sanchez AD, Udeshi ND, Svinkina T, Carr SA, et al. Efficient
846 proximity labeling in living cells and organisms with TurboID. Nat Biotechnol. 2018;36:
847 880–887. doi:10.1038/nbt.4201
848 15. Qin W, Cho KF, Cavanagh PE, Ting AY. Deciphering molecular interactions by
849 proximity labeling. Nat Methods. 2021;18: 133–143. doi:10.1038/s41592-020-01010-5
850 16. Shinoda N, Hanawa N, Chihara T, Koto A, Miura M. Dronc-independent basal
851 executioner caspase activity sustains Drosophila imaginal tissue growth. Proc Natl Acad
852 Sci U S A. 2019;116:20539–20544. doi:10.1073/pnas.1904647116
853 17. Shinoda N, Horikoshi M, Taira Y, Muramoto M, Hirayama S, Murata S, et al. Caspase
854 cleaves Drosophila BubR1 to modulate spindle assembly checkpoint function and
855 lifespan of the organism. FEBS J. 2023;290:4147–4371. doi:10.1111/febs.16811
856 18. Chiba A, Snow P, Keshishian H, Hotta Y. Fasciclin III as a synaptic target recognition
857 molecule in Drosophila. Nature. 1995;374: 166–168. doi:10.1038/374166a0

858 19. Kose H, Rose D, Zhu X, Chiba A. Homophilic synaptic target recognition mediated by
859 immunoglobulin-like cell adhesion molecule Fasciclin III. Development. 1997;124:
860 4143–4152. doi: 10.1242/dev.124.20.4143.
861 20. Tang HL, Tang HM, Fung MC, Hardwick JM. In vivo Caspase tracker biosensor system
862 for detecting anastasis and non-apoptotic caspase activity. Sci Rep. 2015;5: 9015.
863 doi:10.1038/srep09015
864 21. Ding AX, Sun G, Argaw YG, Wong JO, Easwaran S, Montell DJ. CasExpress reveals
865 widespread and diverse patterns of cell survival of caspase-3 activation during
866 development in vivo. Elife. 2016;5: e10936. doi:10.7554/eLife.10936
867 22. Chihara T, Kitabayashi A, Morimoto M, Takeuchi K, Masuyama K, Tonoki A, et al.
868 Caspase Inhibition in Select Olfactory Neurons Restores Innate Attraction Behavior in
869 Aged Drosophila. PLoS Genet. 2014;10: e1004437. doi:10.1371/journal.pgen.1004437
870 23. Hay BA, Wassarman DA, Rubin GM. Drosophila homologs of baculovirus inhibitor of
871 apoptosis proteins function to block cell death. Cell. 1995;83: 1253–1262.
872 doi:10.1016/0092-8674(95)90150-7
873 24. Ditzel M, Broemer M, Tenev T, Bolduc C, Lee T V., Rigbolt KTG, et al. Inactivation of
874 Effector Caspases through Nondegradative Polyubiquitylation. Mol Cell. 2008;32: 540–
875 553. doi:10.1016/j.molcel.2008.09.025
876 25. Lee T V., Fan Y, Wang S, Srivastava M, Broemer M, Meier P, et al. Drosophila IAP1-
877 mediated ubiquitylation controls activation of the initiator caspase DRONC independent
878 of protein degradation. PLoS Genet. 2011;7: e1002261.
879 doi:10.1371/journal.pgen.1002261
880 26. Semmelhack JL, Wang JW. Select Drosophila glomeruli mediate innate olfactory
881 attraction and aversion. Nature. 2009;459: 218–223. doi:10.1038/nature07983

882 27. Walsh JG, Cullen SP, Sheridan C, Lüthi AU, Gerner C, Martin SJ. Executioner caspase-
883 3 and caspase-7 are functionally distinct proteases. Proc Natl Acad Sci U S A. 2008;105:
884 12815–12819. doi:10.1073/pnas.0707715105
885 28. Boucher D, Blais V, Denault JB. Caspase-7 uses an exosite to promote poly(ADP ribose)
886 polymerase 1 proteolysis. Proc Natl Acad Sci U S A. 2012;109: 5669–5674.
887 doi:10.1073/pnas.1200934109
888 29. Desroches A, Denault JB. Caspase-7 uses RNA to enhance proteolysis of poly(ADP-
889 ribose) polymerase 1 and other RNA-binding proteins. Proc Natl Acad Sci U S A.
890 2019;116: 21521–21528. doi:10.1073/pnas.1909283116
891 30. Takemoto K, Nagai T, Miyawaki A, Miura M. Spatio-temporal activation of caspase
892 revealed by indicator that is insensitive to environmental effects. J Cell Biol. 2003;160:
893 235–243. doi:10.1083/jcb.200207111
894 31. Valente P, Lignani G, Medrihan L, Bosco F, Contestabile A, Lippiello P, et al. Cell
895 adhesion molecule L1 contributes to neuronal excitability regulating the function of
896 voltage-gated Na+ channels. J Cell Sci. 2016;129: 1878–1891. doi:10.1242/jcs.182089
897 32. Mukherjee A, Williams DW. More alive than dead: Non-apoptotic roles for caspases in
898 neuronal development, plasticity and disease. Cell Death Differ. 2017;24: 1411–1421.
899 doi:10.1038/cdd.2017.64
900 33. Dehkordi MH, Munn RGK, Fearnhead HO. Non-Canonical Roles of Apoptotic Caspases
901 in the Nervous System. Front Cell Dev Biol. 2022;10: 840023.
902 doi:10.3389/fcell.2022.840023
903 34. Gu Q, Jiao S, Duan K, Wang YX, Petralia RS, Li Z. The BAD-BAX-Caspase-3 Cascade
904 Modulates Synaptic Vesicle Pools via Autophagy. J Neurosci. 2021;41: 1174–1190.
905 doi:10.1523/JNEUROSCI.0969-20.2020

906 35. Cheriyamkunnel SJ, Rose S, Jacob PF, Blackburn LA, Glasgow S, Moorse J, et al. A
907 neuronal mechanism controlling the choice between feeding and sexual behaviors in
908 Drosophila. Curr Biol. 2021;31: 4231-4245.e4. doi:10.1016/j.cub.2021.07.029
909 36. Dorstyn L, Colussi PA, Quinn LM, Richardson H, Kumar S. DRONC, an ecdysone-
910 inducible Drosophila caspase. Proc Natl Acad Sci U S A. 1999;96: 4307–4312.
911 doi:10.1073/pnas.96.8.4307
912 37. Verghese S, Bedi S, Kango-Singh M. Hippo signalling controls Dronc activity to
913 regulate organ size in Drosophila. Cell Death Differ. 2012;19: 1664–1676.
914 doi:10.1038/cdd.2012.48
915 38. Westphal D, Sytnyk V, Schachner M, Leshchyns'ka I. Clustering of the neural cell
916 adhesion molecule (NCAM) at the neuronal cell surface induces caspase-8- and -3-
917 dependent changes of the spectrin meshwork required for NCAM-mediated neurite
918 outgrowth. J Biol Chem. 2010;285: 42046–42057. doi:10.1074/jbc.M110.177147
919 39. Luck K, Kim DK, Lambourne L, Spirohn K, Begg BE, Bian W, et al. A reference map
920 of the human binary protein interactome. Nature. 2020;580: 402–408.
921 doi:10.1038/s41586-020-2188-x
922 40. Li L, Ding Z, Pang TL, Zhang B, Li CH, Liang AM, et al. Defective minor spliceosomes
923 induce SMA-associated phenotypes through sensitive intron-containing neural genes in
924 Drosophila. Nat Commun. 2020;11: 5608. doi:10.1038/s41467-020-19451-z
925 41. Koto A, Kuranaga E, Miura M. Temporal regulation of Drosophila IAP1 determines
926 caspase functions in sensory organ development. J Cell Biol. 2009;187: 219–31.
927 doi:10.1083/jcb.200905110
928 42. Karim MR, Endo K, Moore AW, Taniguchi H. Whole mount immunolabeling of
929 olfactory receptor neurons in the Drosophila antenna. J Vis Exp. 2014;51245.
930 doi:10.3791/51245

931 43. Okuda S, Watanabe Y, Moriya Y, Kawano S, Yamamoto T, Matsumoto M, et al.
932 JPOSTrepo: An international standard data repository for proteomes. Nucleic Acids Res.
933 2017;45: D1107–D1111. doi:10.1093/nar/gkw1080
934 44. Huang DW, Sherman BT, Lempicki RA. Bioinformatics enrichment tools: Paths toward
935 the comprehensive functional analysis of large gene lists. Nucleic Acids Res. 2009;37:
936 1–13. doi:10.1093/nar/gkn923
937 45. Deluca SZ, Spradling AC. Efficient expression of genes in the drosophila germline using
938 a uas promoter free of interference by hsp70 pirnas. Genetics. 2018;209: 381–387.
939 doi:10.1534/genetics.118.300874
940 46. Kashio S, Obata F, Zhang L, Katsuyama T, Chihara T, Miura M. Tissue nonautonomous
941 effects of fat body methionine metabolism on imaginal disc repair in Drosophila. Proc
942 Natl Acad Sci U S A. 2016;113: 1835–1840. doi:10.1073/pnas.1523681113
943

944 **Figures & Figure Legends**

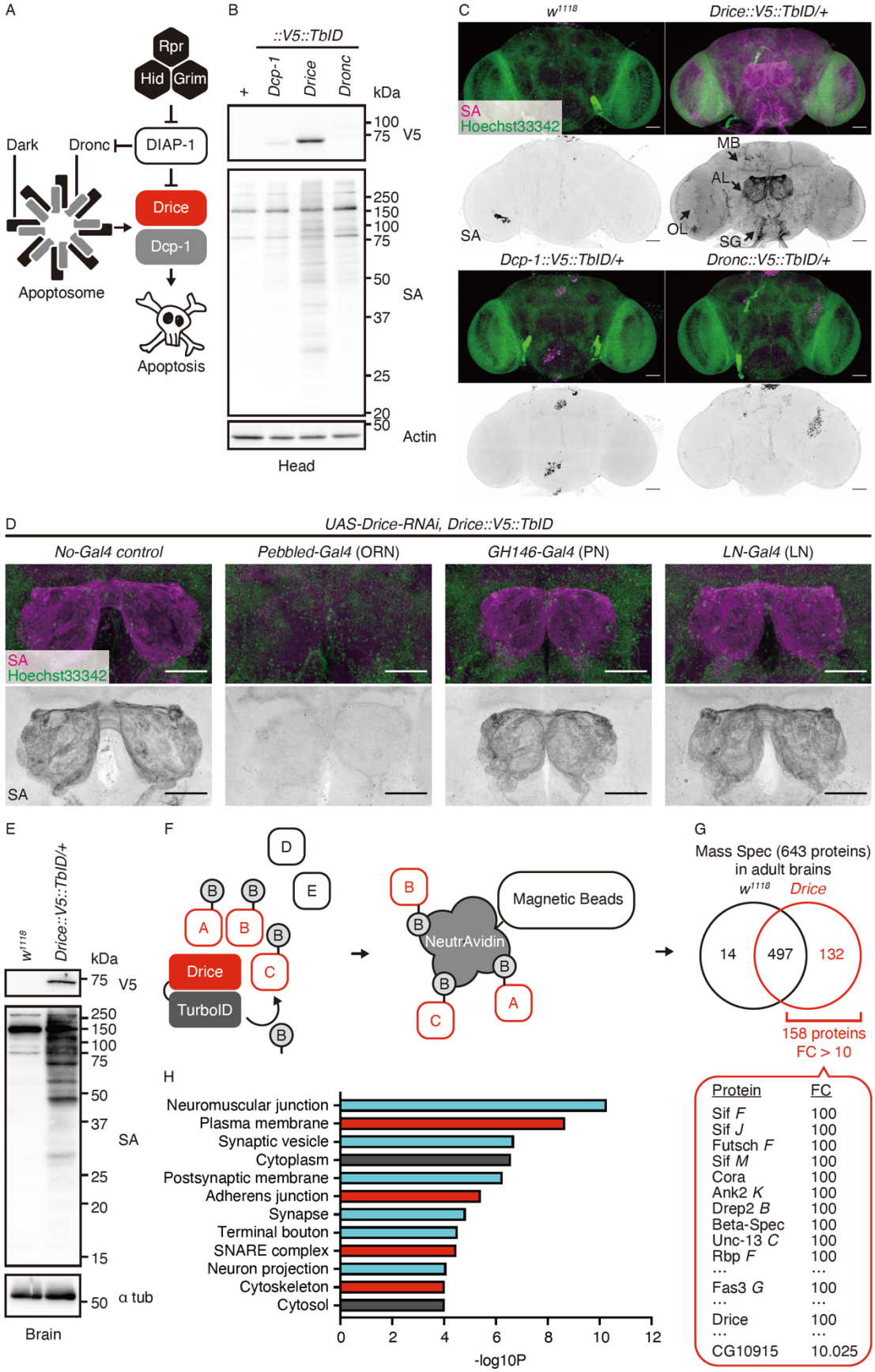

945

946 **Fig 1. Expression patterns and proximal proteins of Drice in the adult brain.**

947 (A) Schematic diagram of *Drosophila* apoptosis signaling. (B) Western blot of expression of
948 caspases in adult male heads. (C) Representative images of adult male brains. Expression
949 patterns of each caspase are visualized using Streptavidin (SA, magenta). Nuclei are visualized
950 by Hoechst33342 (Green). Scale bar: 50 μm. (D) Representative images of antennal lobes (ALs)
951 in the adult female brains. Expression patterns of Drice are visualized using SA (magenta).
952 Nuclei are visualized by Hoechst33342 (Green). Scale bar: 50 μm. (E) Western blot of proteins
953 extracted from adult male brains. (F) Schematic diagram of the TurboID-mediated
954 identification of proximal proteins. (G) A summary of mass spectrometry analysis of proteins
955 of the adult male brains. Partial list of Drice proximal proteins and their Fold Change (FC) are
956 shown. (H) Gene Ontology analysis (Cellular Compartment) of 158 Drice proximal proteins
957 (*Drice::V5::TurboID/w*^{1118} > 10). Cyan: neural-related fraction, Red: membrane fraction.

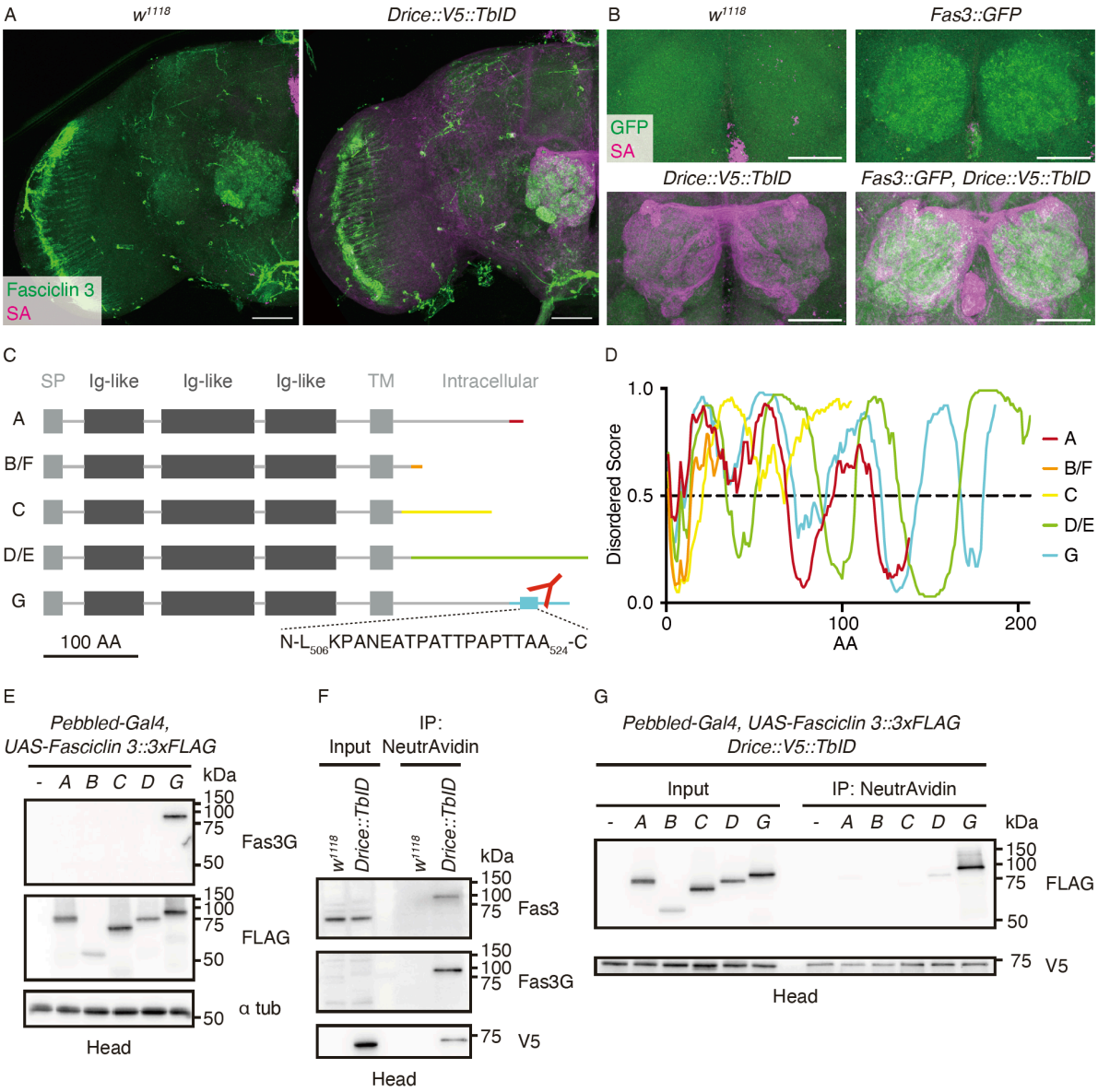

958

959 **Fig 2. A specific isoform of Fasciclin 3 is in proximity to Drice.**

960 (A) Representative expression patterns of Drice (Streptavidin (SA); magenta) and Fasciclin 3
961 (Fas3, anti-Fasciclin 3 antibody staining; green) in the adult male brains. Scale bar: 50 μm. (B)
962 Representative expression patterns of Drice (SA; magenta) and Fas3 (anti-GFP antibody
963 staining; green) in the antennal lobes (ALs) of the adult male brains. Scale bar: 50 μm. (C)
964 Schematic protein structures of Fas3 isoforms. Intracellular regions differ from each other. A
965 peptide region used to raise anti-Fas3G antibody is shown. (D) IDR predictions of intracellular
966 regions of each protein isoform. (E) Western blot of proteins extracted from adult heads. Anti-
967 Fas3G antibody specifically detects Fas3 isoform G. (F) Western blot of adult male heads. Drice

968 proximal proteins were purified using NeturAvidin. (G) Western blot of adult head proteins.

969 Drice proximal proteins were purified using NeturAvidin.

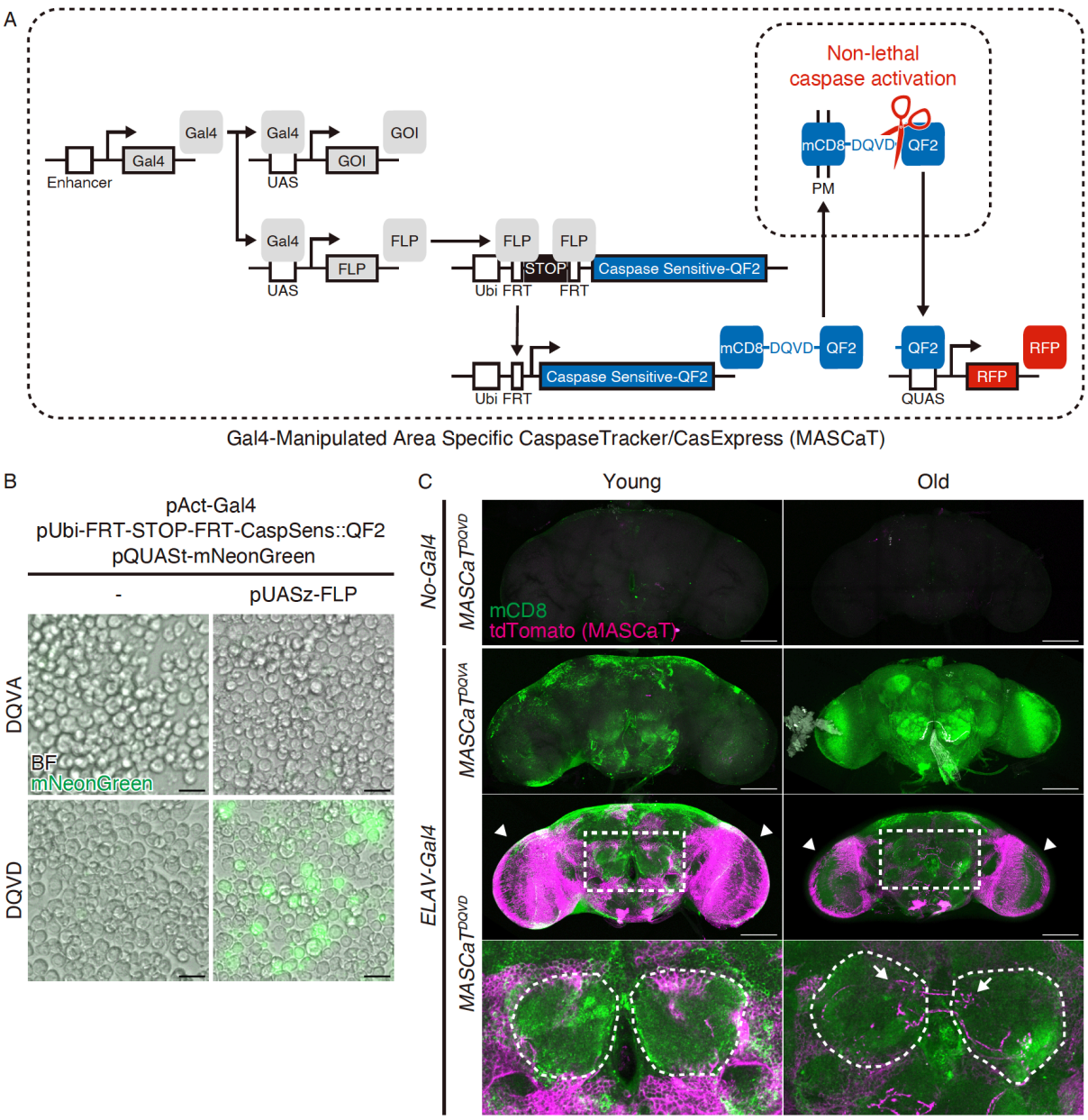

970

971 **Fig 3. A Gal4-Manipulated Area Specific CaspaseTracker/CasExpress (MASCaT).**

972 (A) A schematic diagram of MASCaT expressed using the Gal4/UAS system with FLP-
973 mediated recombination. Caspase sensitive-QF2 is activated by caspase-mediated cleavage at
974 the plasma membrane. (B) Representative images of S2 cells expressing caspase sensitive-QF2
975 probes by the Gal4/UAS system with FLP-mediated recombination. Scale bar: 20 μm. (C)
976 Representative images of adult male brains of young (1 week old) and old (3 weeks old) flies
977 raised at 29°C. Arrowheads indicate optic lobes. Magnified images (white rectangle) show

978 antennal lobes (ALs; white circles). Arrows indicate age-dependent caspase activation at the

979 ALs. Scale bar: 100 μm.

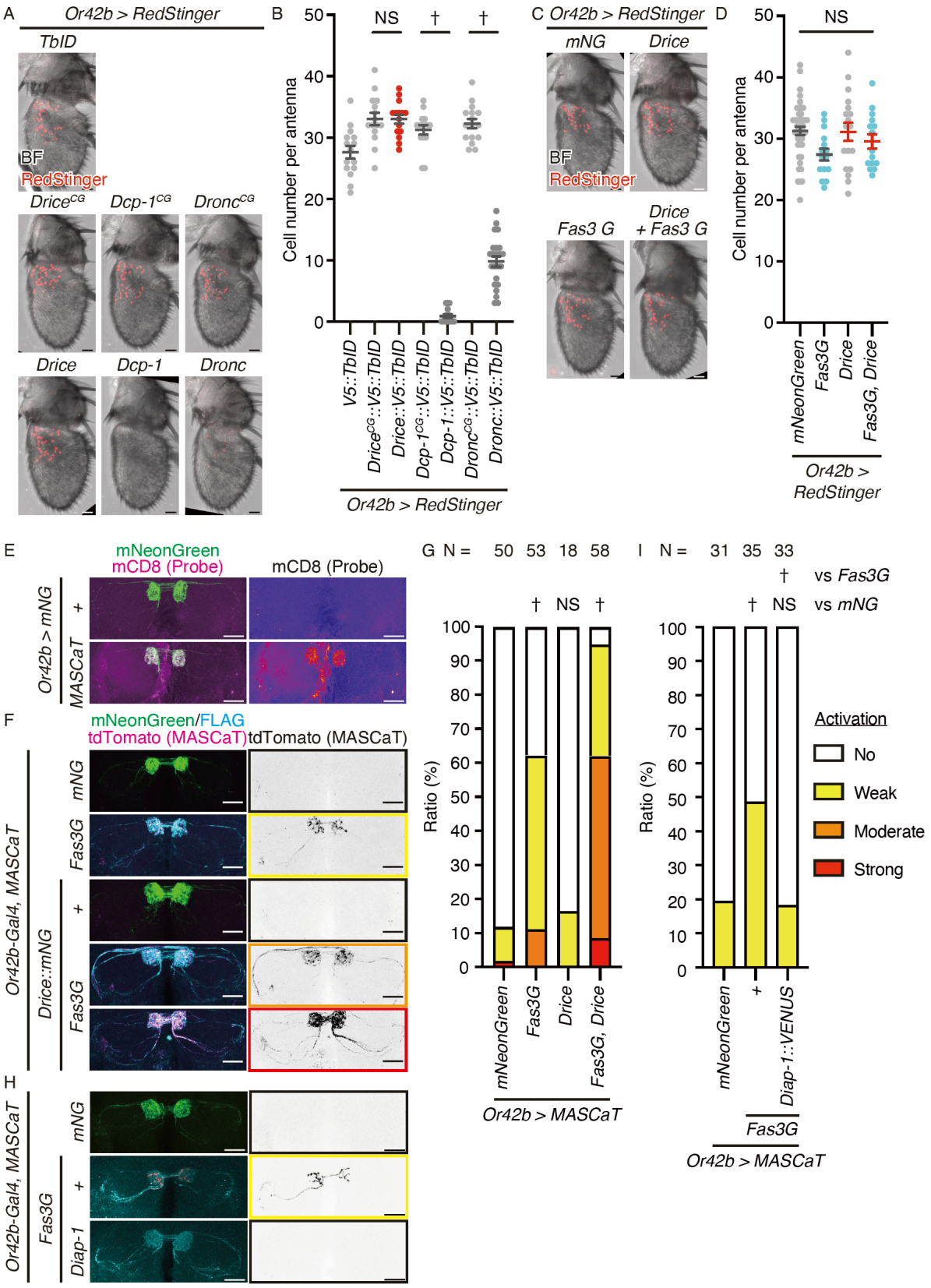

980

981 **Fig 4. *Fasciclin 3 isoform G* overexpression enhances non-lethal caspase activation.**

982 (A) Representative images of the adult male antennae of 1 weeks old flies raised at 29°C. Cell
983 bodies are visualized using RedStinger (red). Scale bar: 20 μm. (B) Quantification of cell
984 number of (A). Data are presented as mean ± SEM. *P*-values were calculated using one-way
985 analysis of variance (ANOVA) with Bonferroni's correction for selected pairs. NS: $P > 0.05$,
986 †: $P < 0.05$. (C) Representative images of the adult male antennae of 1 week old flies raised at
987 29°C. Cell bodies are visualized using RedStinger (red). Scale bar: 20 μm. (D) Quantification
988 of cell number of (C). Data are presented as mean ± SEM. *P*-values were calculated using one-
989 way ANOVA with Bonferroni's correction for every pair. NS: $P > 0.05$, †: $P < 0.05$. (E)
990 Representative images of the antennal lobes (ALs) of male brains of 1 week old flies raised at
991 29°C expressing MASCaT probe (mCD8). Scale bar: 30 μm. (F) Representative images of the
992 ALs of brains of 1 week old flies raised at 29°C with caspase activation visualized by MASCaT.
993 Scale bar: 30 μm. (G) Quantifications of caspase activity detected by MASCaT of (F). *P*-values
994 were calculated using chi-square test with Bonferroni's correction using mNeonGreen as
995 control. NS: $P > 0.05$, †: $P < 0.05$. Sample sizes are shown in the graph. (H) Representative
996 images of the ALs of brains of 1 week old flies raised at 29°C with caspase activation visualized
997 by MASCaT. Scale bar: 30 μm. (I) Quantifications of caspase activity detected by MASCaT of
998 (H). *P*-values were calculated using chi-square test with Bonferroni's correction using
999 mNeonGreen and Fas3G as controls, respectively. NS: $P > 0.05$, †: $P < 0.05$. Sample sizes are
1000 shown in the graph.

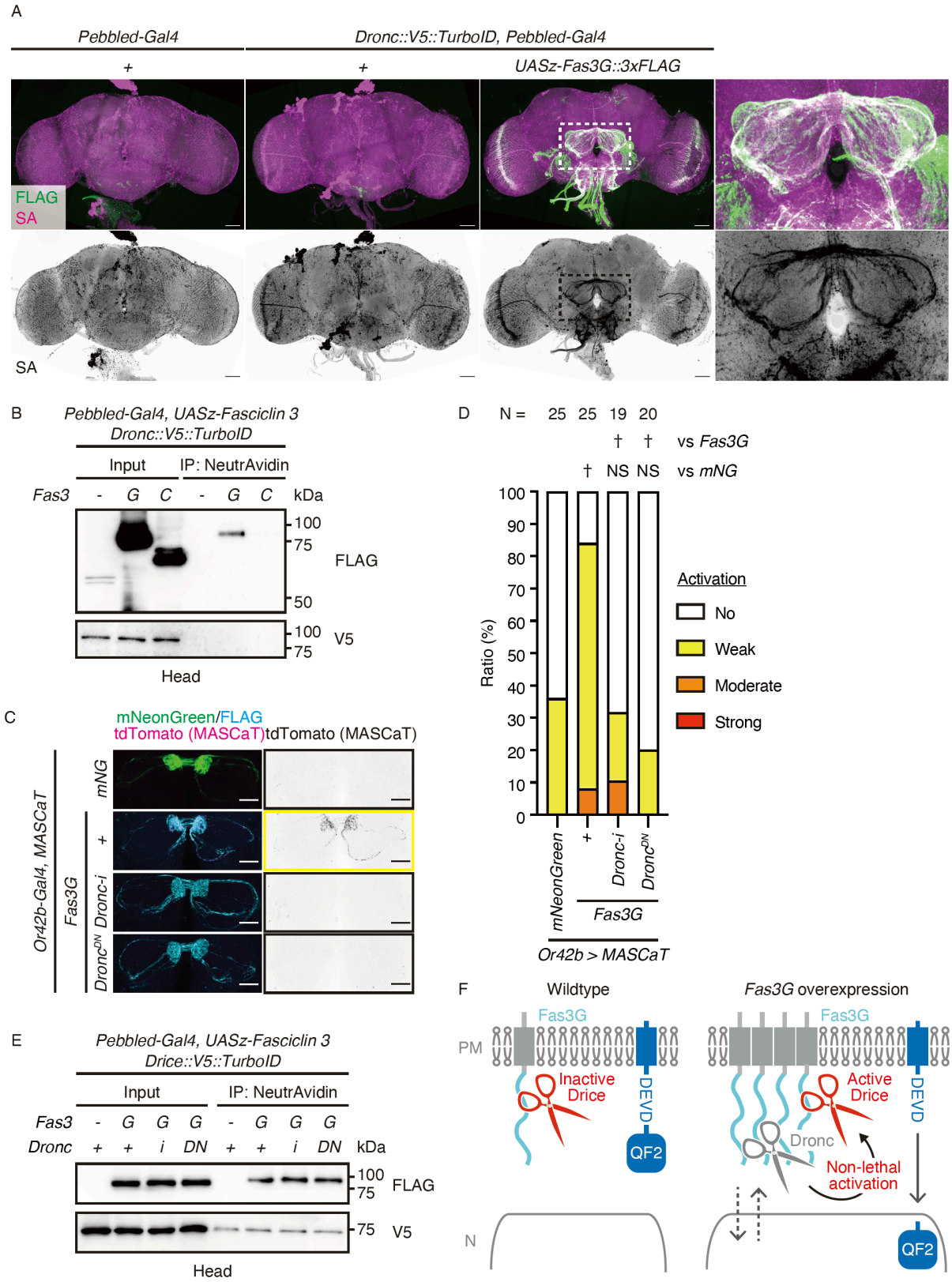

1001

1002 **Fig 5. *Fasciclin 3 isoform G* overexpression enhances non-lethal caspase activation in a**

1003 **Dronc-dependent manner.**

1004 (A) Representative images of adult male brains. Expression patterns of Dronc are visualized
1005 using Streptavidin (SA, magenta). Magnified images (white rectangle) show antennal lobes
1006 (ALs). Scale bar: 50 μm. (B) Western blot of adult male heads. Dronc proximal proteins were
1007 purified using NeturAvidin. (C) Representative images of the AL of brains of 1 week old flies
1008 raised at 29°C with caspase activation visualized using MASCaT. Scale bar: 30 μm. (D)
1009 Quantifications of caspase activity detected using MASCaT of (C). *P*-values were calculated
1010 using chi-square test with Bonferroni's correction using mNeonGreen and Fas3G as controls,
1011 respectively. NS: $P > 0.05$, †: $P < 0.05$. Sample sizes are shown in the graph. (E) Western blot
1012 of adult male heads. Drice proximal proteins were purified using NeturAvidin. (F) A schematic
1013 model of subcellularly restricted non-lethal caspase activation upon Fas3G overexpression.

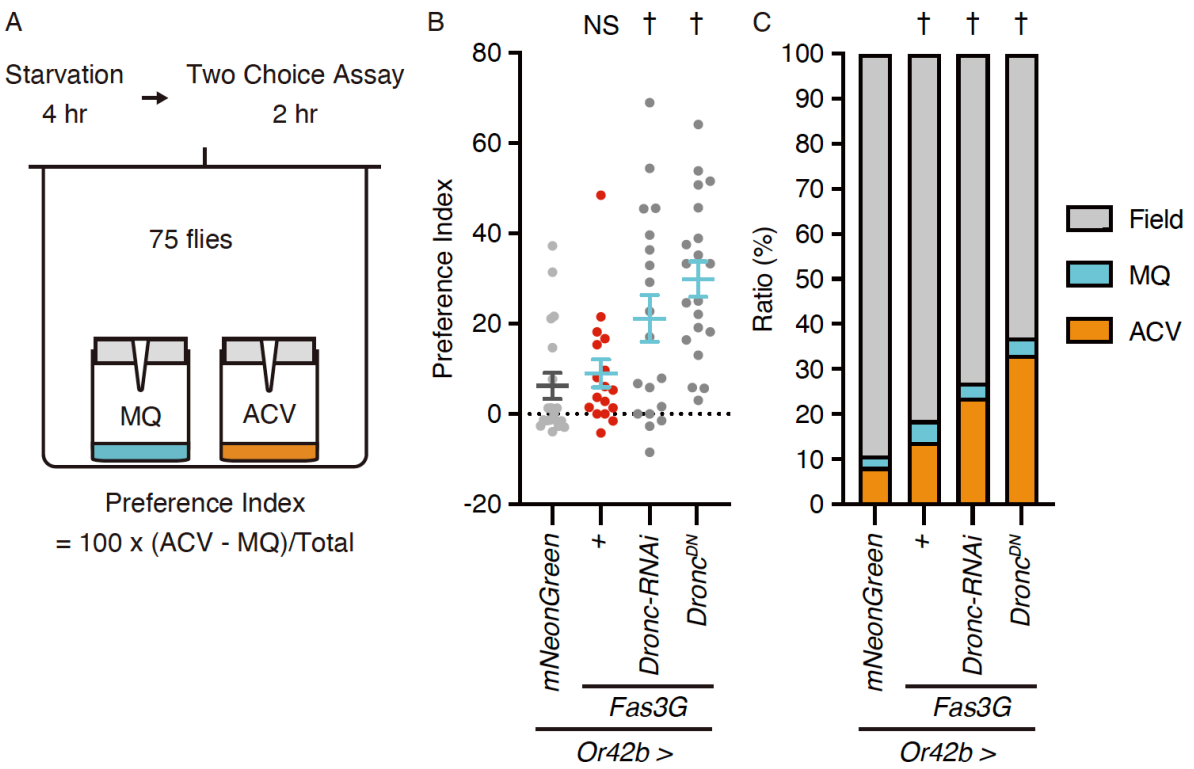

1014

1015 **Fig 6. *Fasciclin 3 isoform G* overexpression-facilitated caspase activation regulates**

1016 **attraction behavior.**

1017 (A) Schematic diagram of two choice preference assay. Flies are starved for 4 hours before the

1018 assay. Flies are left for 2 hours in the bottle. Preference index is calculated by counting the

1019 number of flies left in MQ, ACV and other (field) compartments. (B) Preference index of 1

1020 week old male flies raised at 29°C in response to 1% apple cider vinegar in two choice

1021 preference assay. Data are presented as mean ± SEM. *P*-values were calculated using one-way

1022 ANOVA followed by Dunnets' multiple comparison test using mNeonGreen as a control. NS:

1023 $P > 0.05$, †: $P < 0.05$. Sample sizes: mNG (N = 19 (1327 flies)), Fas3G (N = 17 (1191 flies)),

1024 Fas3G + Dronc-RNAi (N = 19 (1295 flies)), Fas3G + $Dronc^{DN}$ (N = 20 (1320 flies)). (C) The

1025 ratio of flies in the given conditions in the two choice preference assay of (A). *P*-values were

1026 calculated using chi-square test with Bonferroni's correction using mNeonGreen as control. †:

1027 $P < 0.05$. Sample sizes: mNG (N = 1327 flies), Fas3G (N = 1191 flies), Fas3G + Dronc-RNAi

1028 (N = 1295 flies), Fas3G + $Dronc^{DN}$ (N = 1320 flies).

1029 **Legends for Figure S1–4**

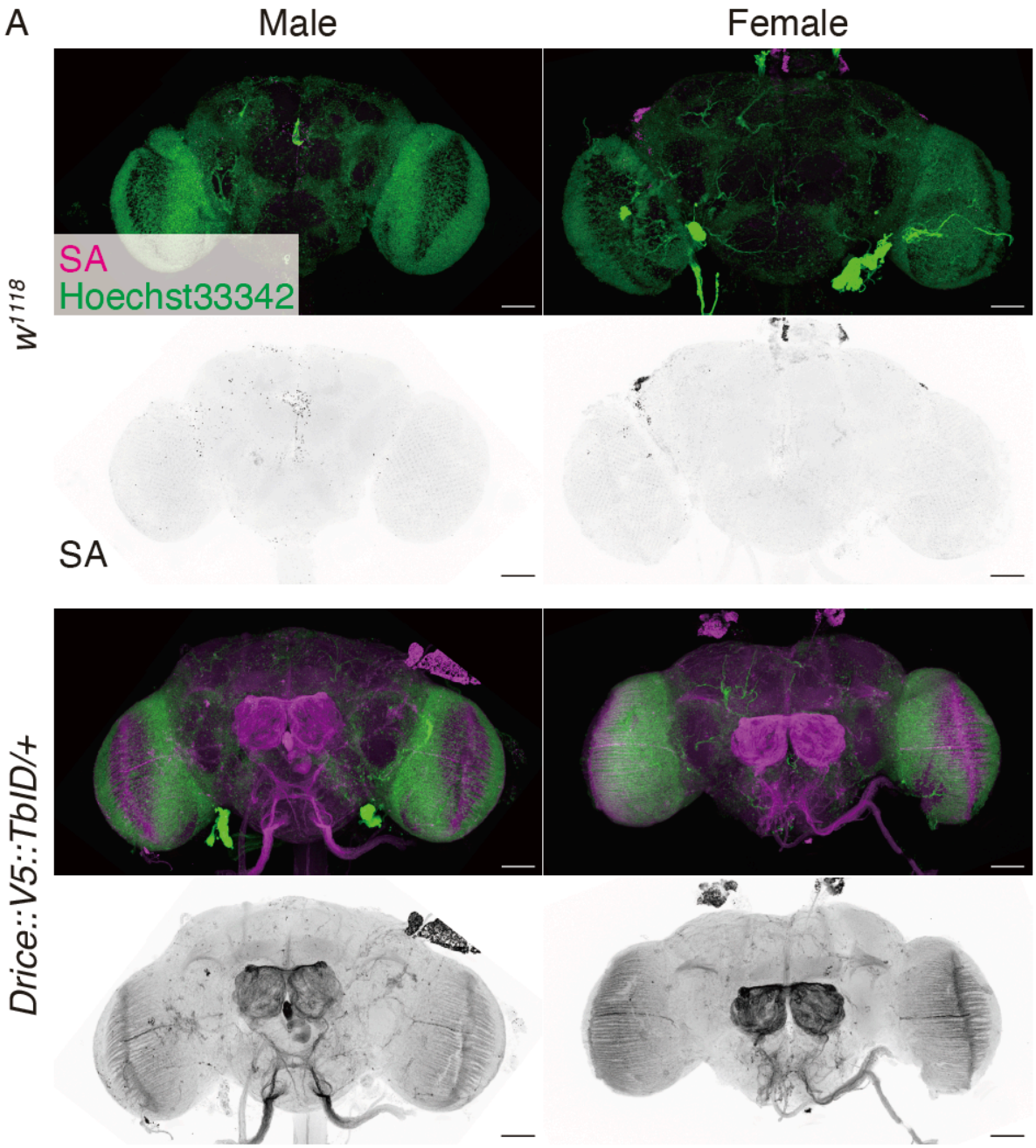

1030

1031 **Fig S1. Expression patterns of Drice in the adult brain in males and females.**

1032 (A) Representative images of adult male and female brains. Expression patterns of Drice are

1033 visualized using Streptavidin (SA, magenta). Nuclei are visualized by Hoechst33342 (Green).

1034 Scale bar: 50 μm.

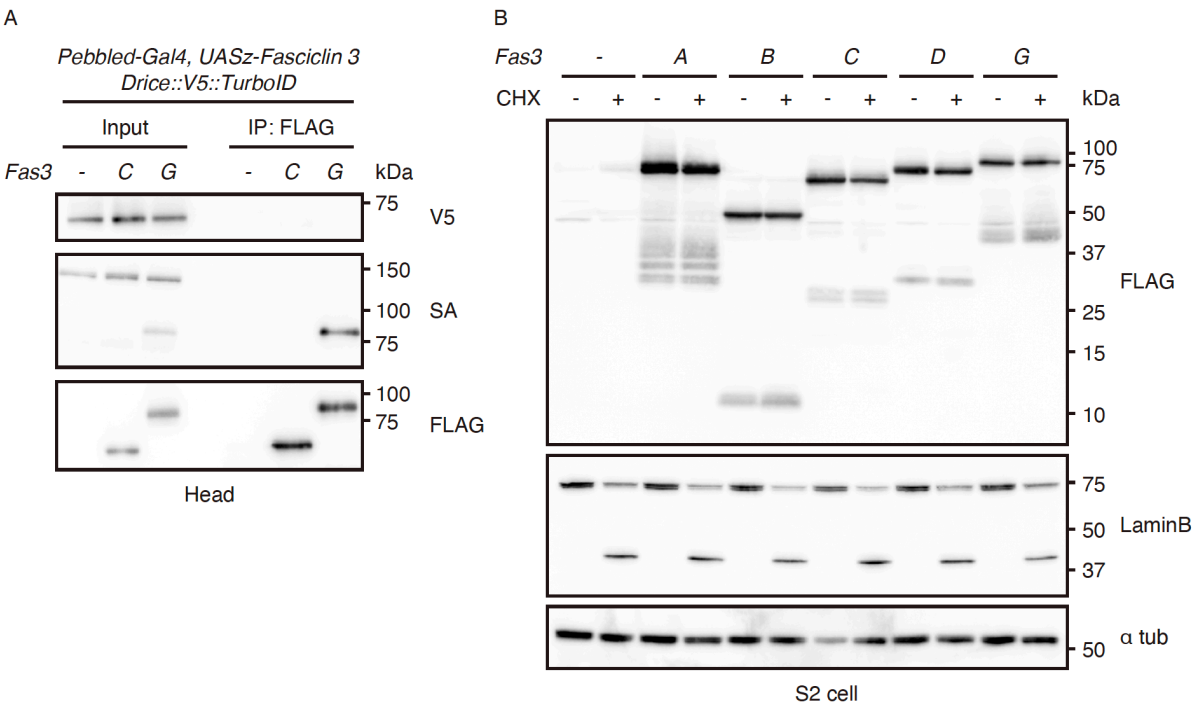

1035

1036 **Fig S2. Biochemical property of Fas3s with caspases.**

1037 (A) Co-immunoprecipitation of 3xFLAG-tagged Fas3s with V5-tagged Drice extracted from

1038 adult male heads. (B) Western blot for 3xFLAG-tagged Fas3s expressed in *Drosophila* S2 cells.

1039 Apoptosis was induced by treating S2 cells with cycloheximide (CHX).

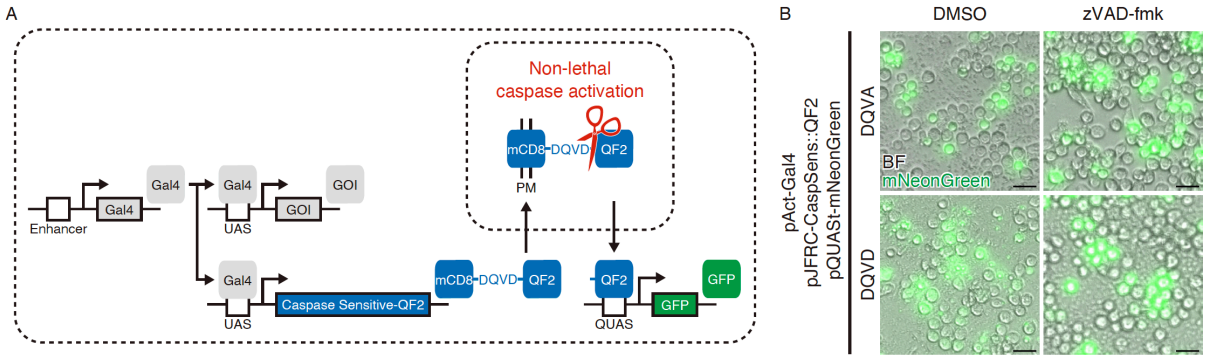

1040

1041 **Fig S3. Overexpression of *mCD8::DQVD::QF2* probes in *Drosophila* S2 cells.**

1042 (A) A schematic diagram of MASCaT expressed directly using the Gal4/UAS system. Caspase

1043 sensitive-QF2 is activated by caspase-mediated cleavage at the plasma membrane. (B)

1044 Representative images of S2 cells expressing caspase sensitive-QF2 probes directly by the

1045 Gal4/UAS system. A pan-caspase inhibitior, zVAD-fmk, is treated to inhibit caspase activity.

1046 Scale bar: 20 μm.

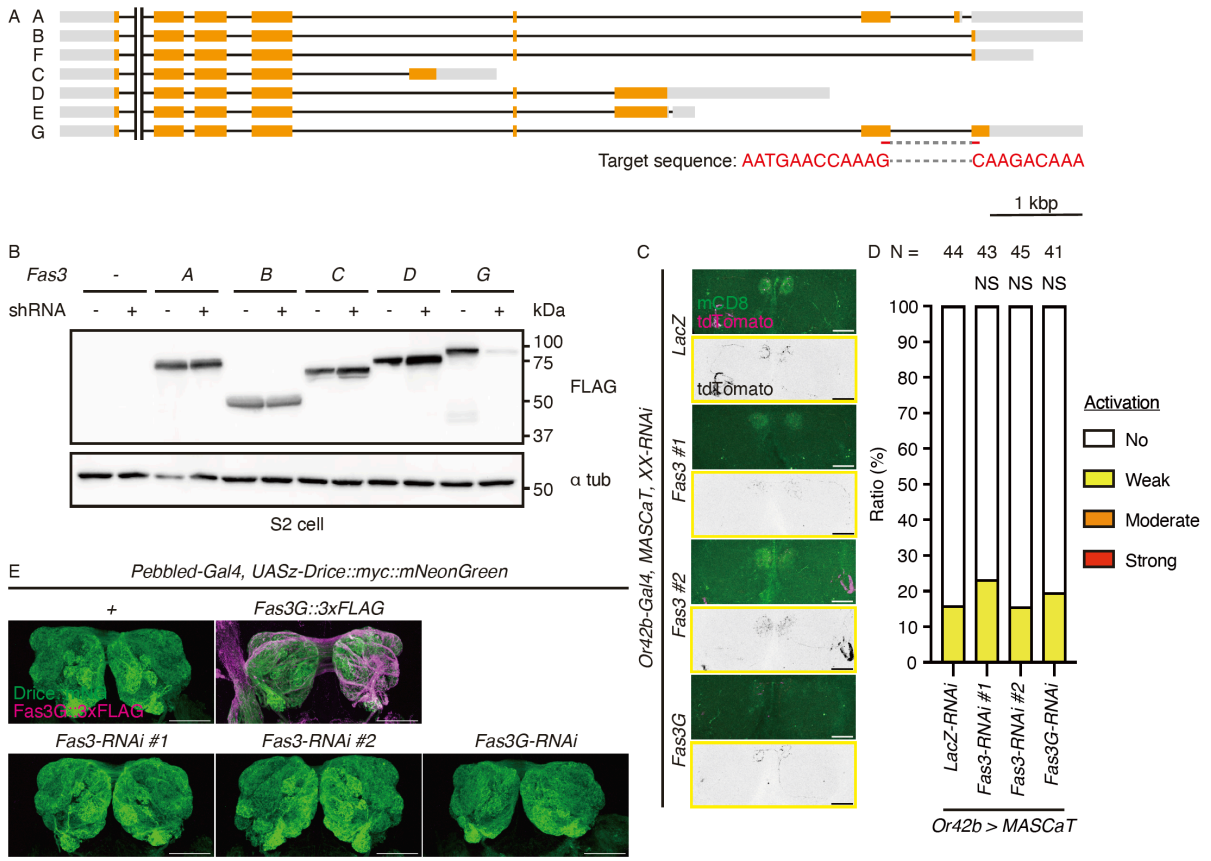

Fig S4. Loss of function analysis of Fas3G.

(A) Gene structure of Fas3. CDS (orange) and UTR (grey) are shown in boxes. Target sequence of Fas3G-shRNA is shown in red. (B) Western blot for 3xFLAG-tagged Fas3s expressed in S2 cells with Fas3G-shRNA. (C) Representative images of the ALs of brains of 1 week old flies raised at 29°C with caspase activation visualized by MASCaT. Scale bar: 30 μm. (D) Quantifications of caspase activity detected by MASCaT of (C). *P*-values were calculated using chi-square test with Bonferroni's correction using *LacZ-RNAi* as control. NS: $P > 0.05$. Sample sizes are shown in the graph. (E) Representative images of the ALs of brains of 1 week old flies expressing mNeonGreen-tagged Drice (green) and 3xFLAG-tagged Fas3G (magenta). Scale bar: 50 μm.

1058 **Legends for Table S1–5**

1059 **Table S1. Proximal protein list.** A list of the identified proximal proteins (Abundance ratio
1060 (Drice::V5::TurboID/Control) > 10). The UniProt Accessions, Gene Description, and
1061 Abundance Ratio (Drice::V5::TurboID/Control) are listed.

1062

1063 **Table S2. Gene Ontology analysis.** The result of Gene Ontology (GO) analysis of Cellular
1064 Compartment for Drice proximal proteins. GO term, P values, Fold Enrichment, Count and
1065 Genes are listed.

1066

1067 **Table S3. LC settings.** Gradient settings for LC analysis are presented.

1068

1069 **Table S4. MS/MS settings.** Settings used for the MS/MS analysis are presented.

1070

1071 **Table S5. Proteome Discoverer 2.2 settings.** Proteome Discoverer 2.2 settings for proteomics
1072 analysis are presented.